The chemical abundance patterns of the most metal-poor stars

Norbert Christlieb
Zentrum für Astronomie (ZAH)
der Universität Heidelberg,
Landessternwarte

RUPRECHT-KARLS-UNIVERSITÄT HEIDELBERG

ZAH

Deutsche Forschungsgemeinschaft DFG

SFB 881
The Milky Way System

Contents

- Introductory remarks
- Wide-angle sky surveys for metal-poor stars
- The abundance patterns of the most metal-poor stars currently known
- Outlook: Kinematics, and Gaia

Chemical enrichment of the Universe

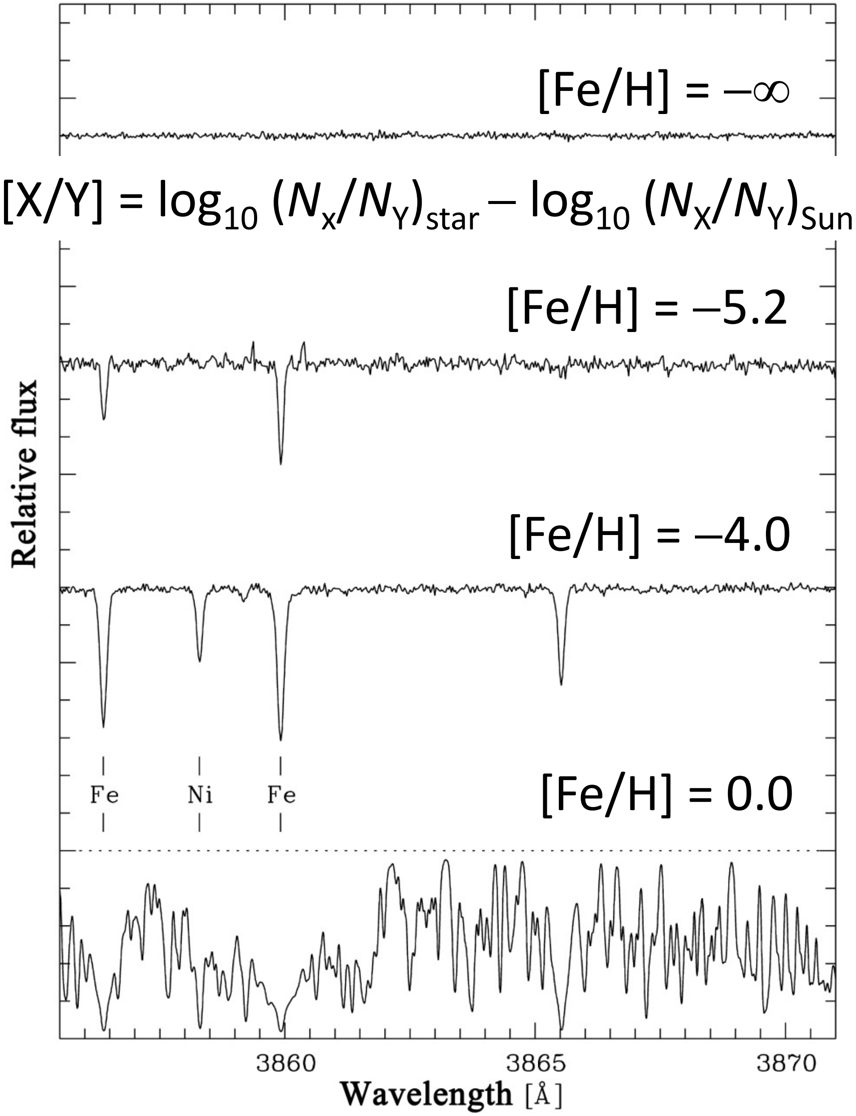

$$[X/Y] = \log_{10}(N_X/N_Y)_{star} - \log_{10}(N_X/N_Y)_{Sun}$$

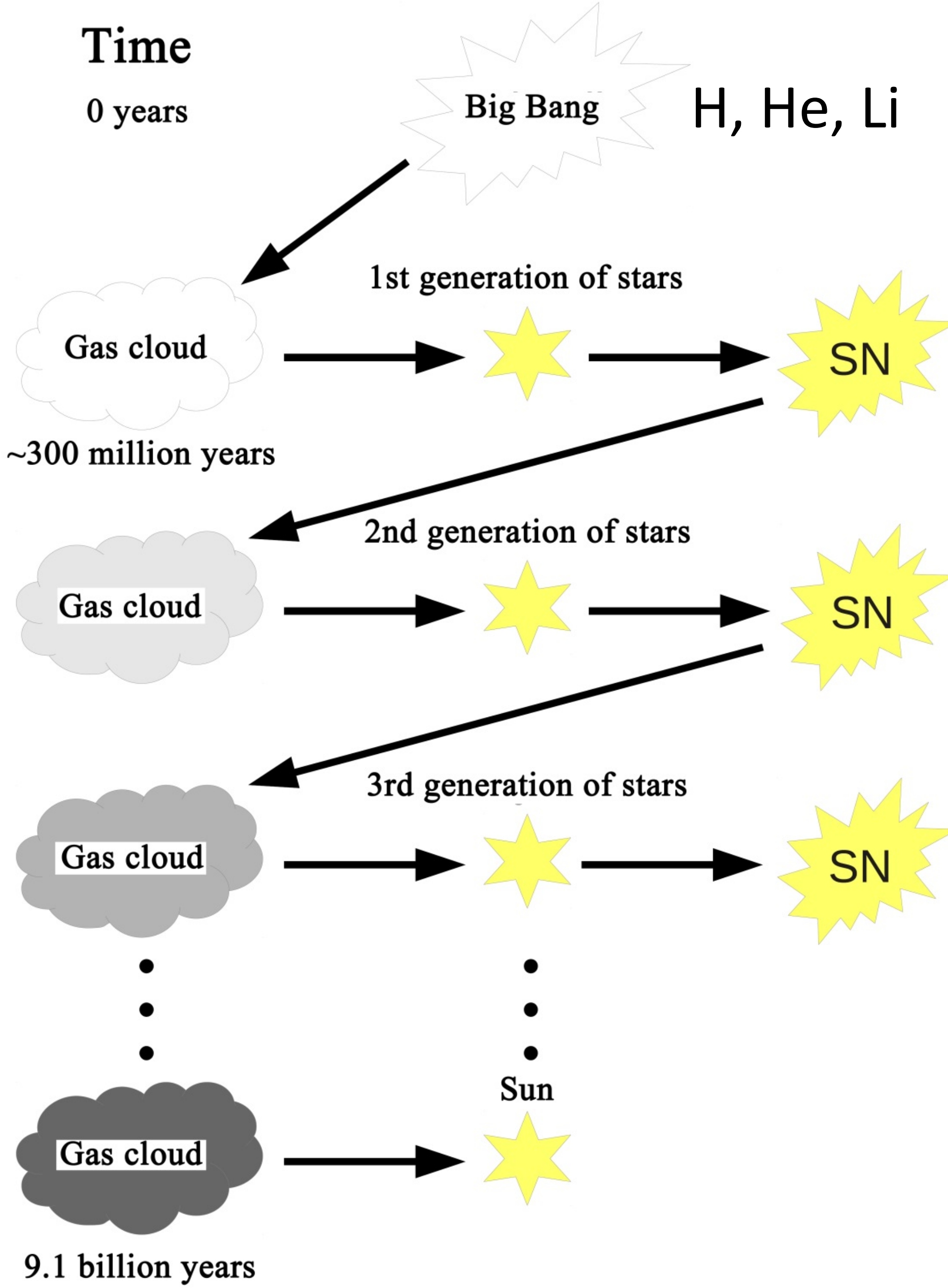

Strongly r-process enhanced stars

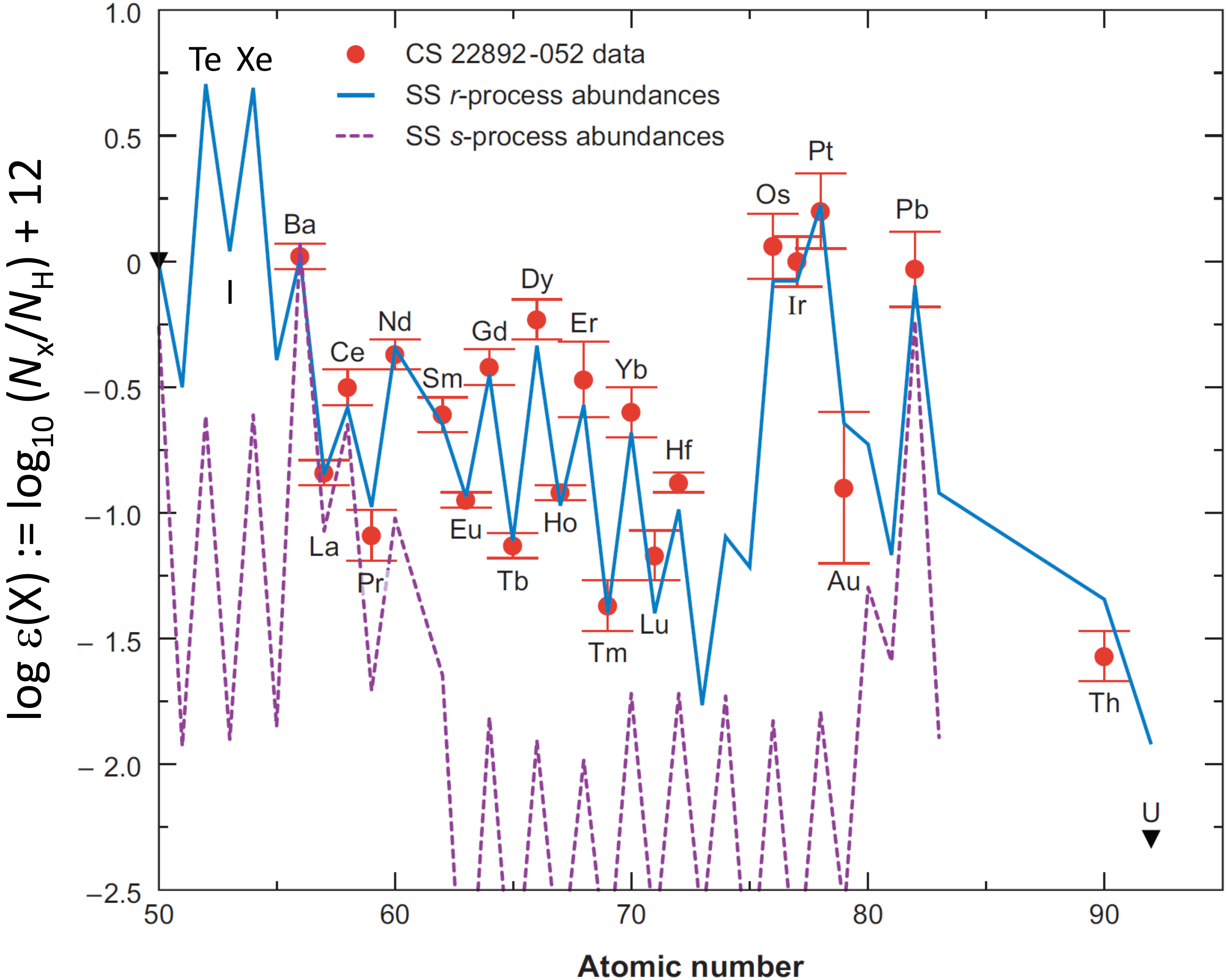

(Sneden et al. 2008, ARA&A 46, 241)

Strongly s-process enhanced stars

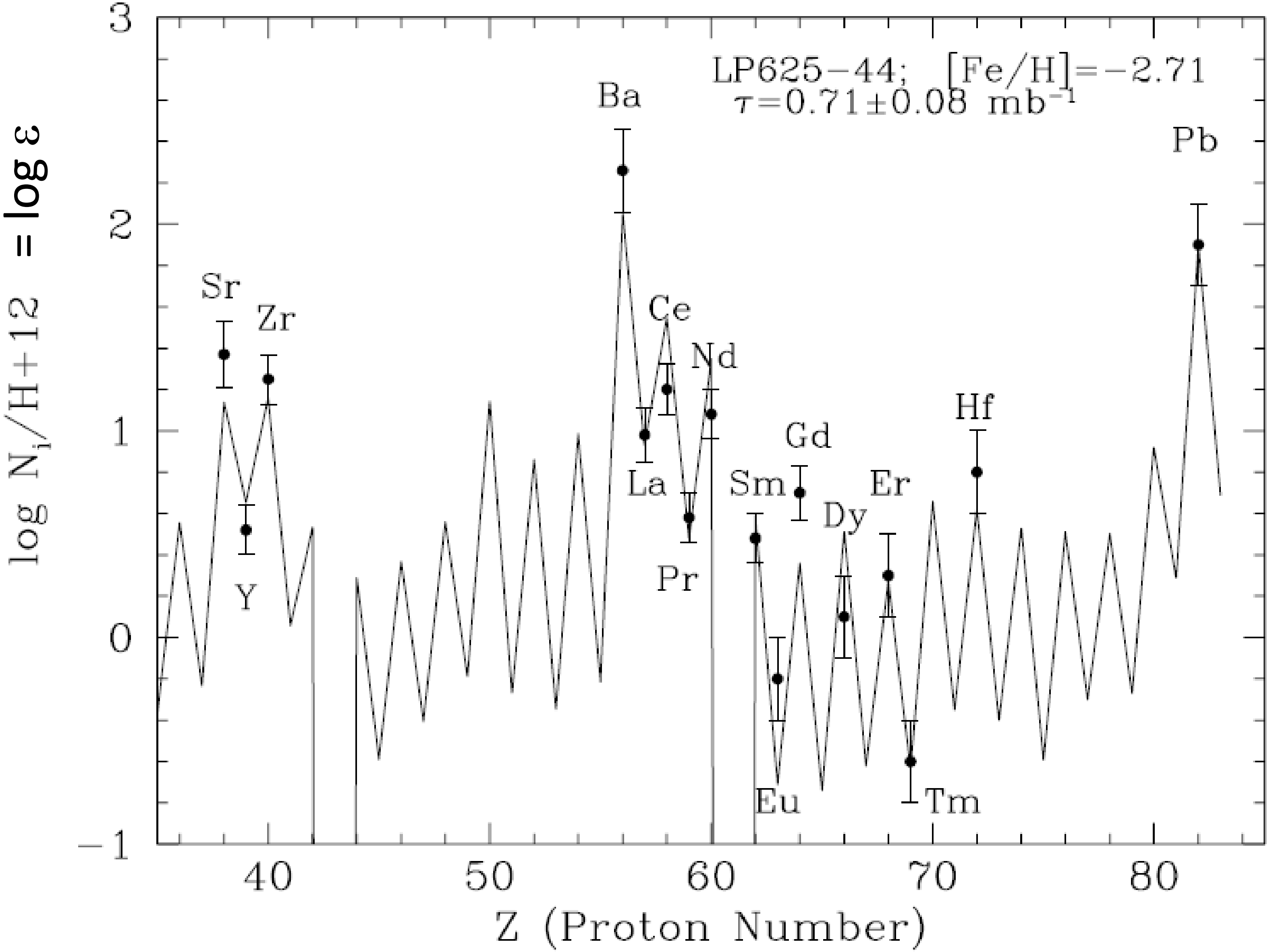

(Aoki et al. 2001, 561, 346)

HD 122563: The prototype LEPP star

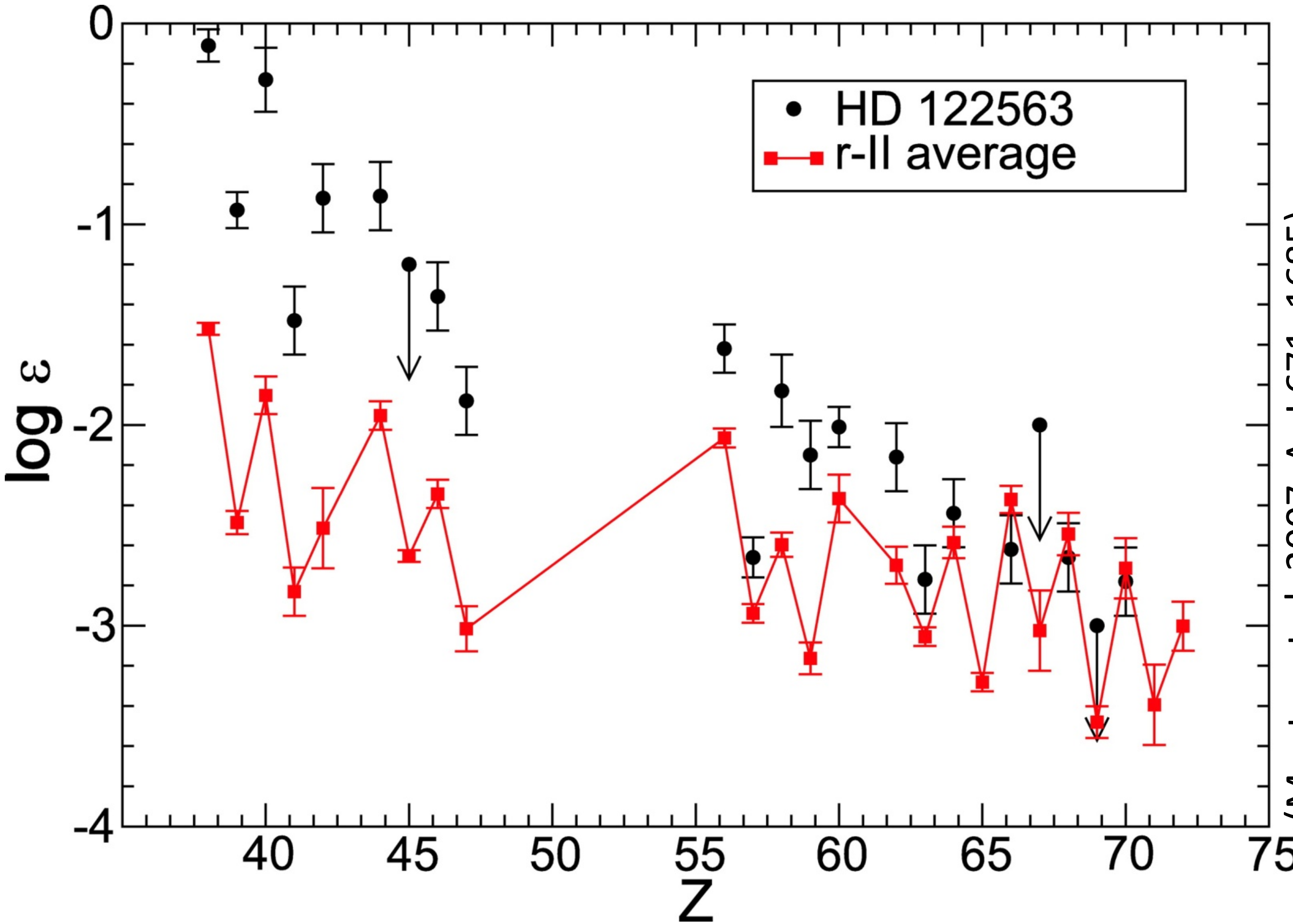

(Montes et al. 2007, ApJ 671, 1685)

Light neutron-capture elements

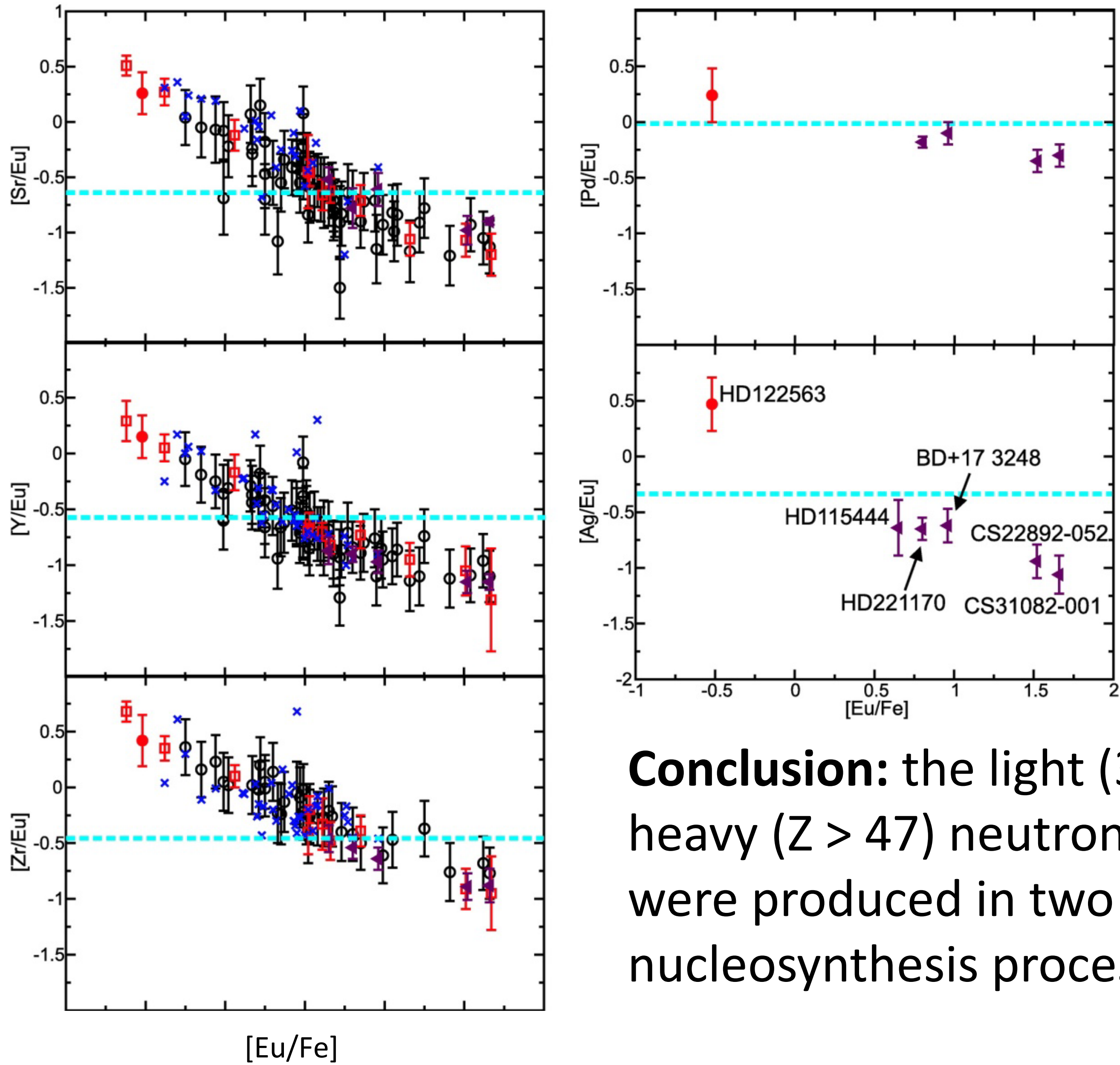

Montes et al. (2007, ApJ 671, 1685)

Conclusion: the light (38 ≤ Z ≤ 47) and heavy (Z > 47) neutron-capture elements were produced in two different nucleosynthesis processes.

Palladium and silver

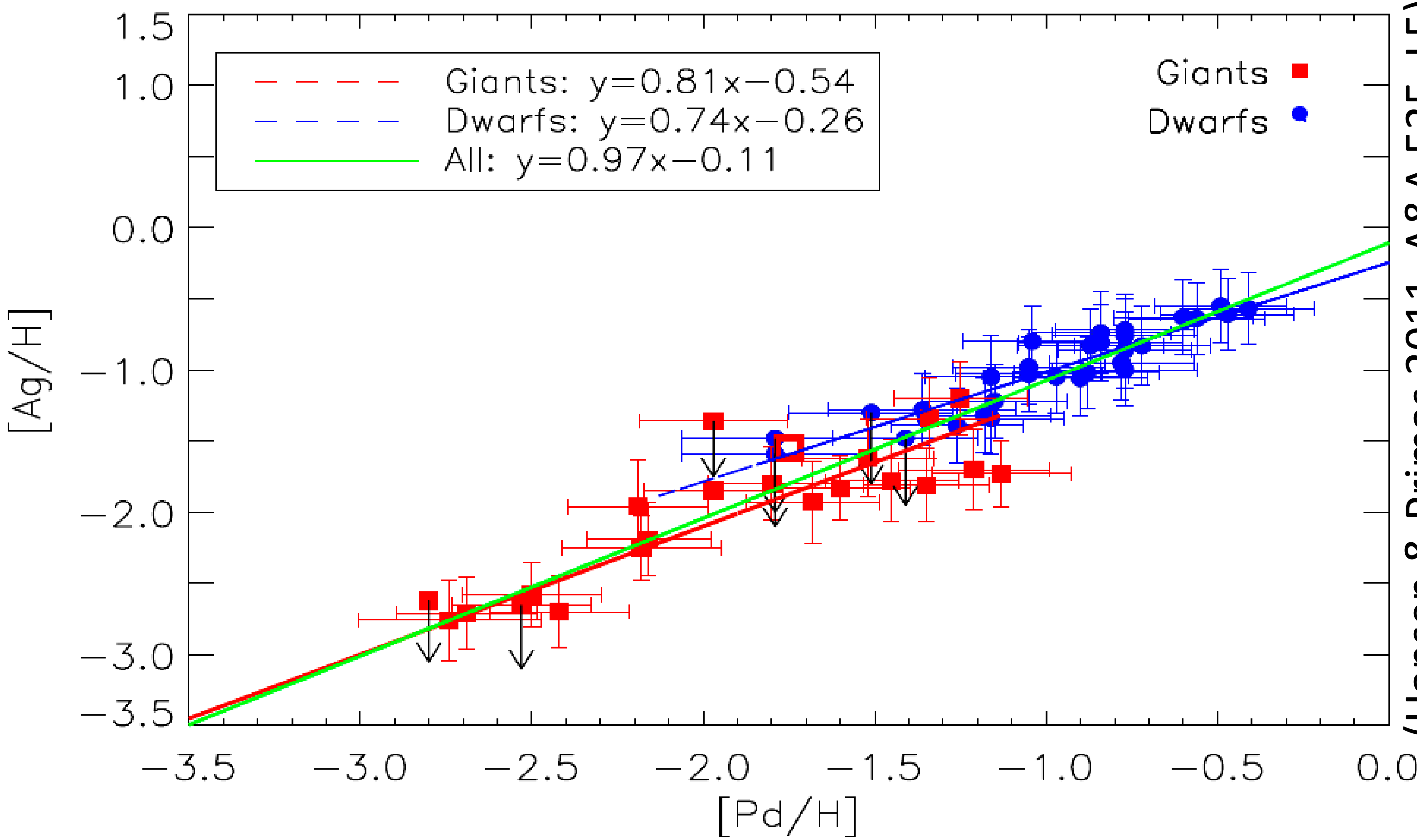

(Hansen & Primas 2011, A&A 525, L5)

⇒ Palladium and silver were produced in the same nucleosynthesis process.

Abundance ratio diagrams

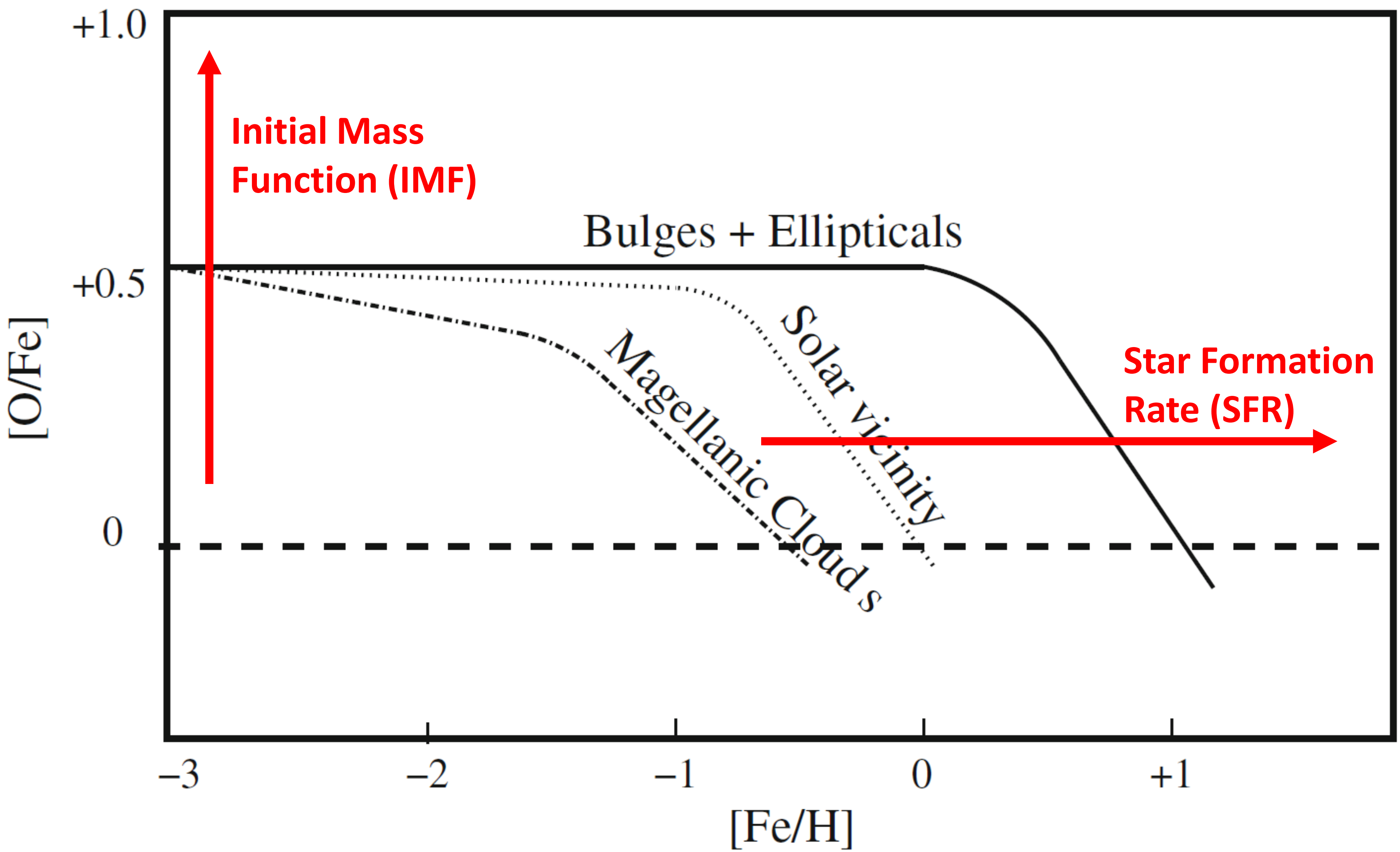

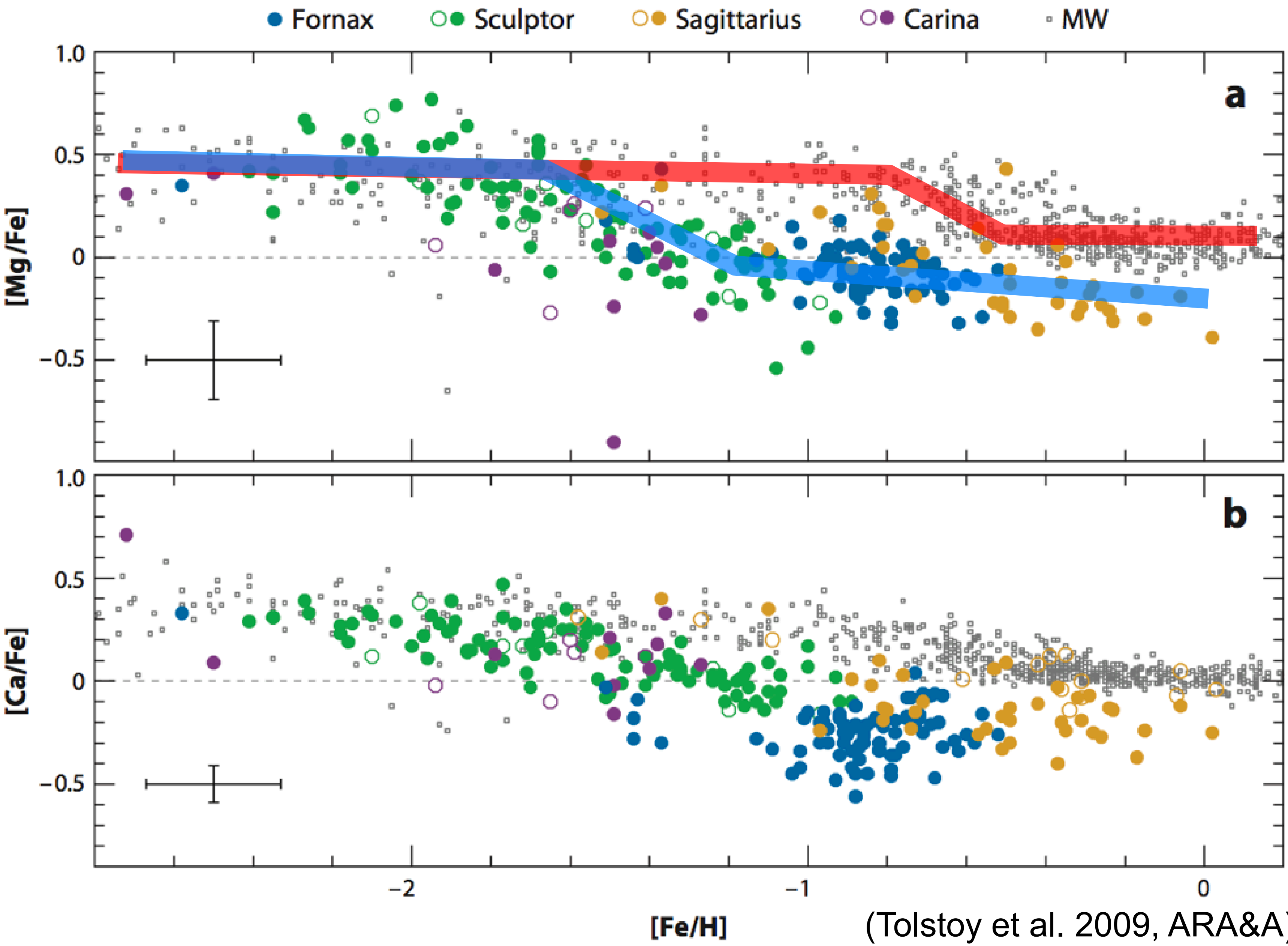

(Tolstoy et al. 2009, ARA&A)


Searches for
metal-poor stars

The metallicity distribution function of the Galactic halo

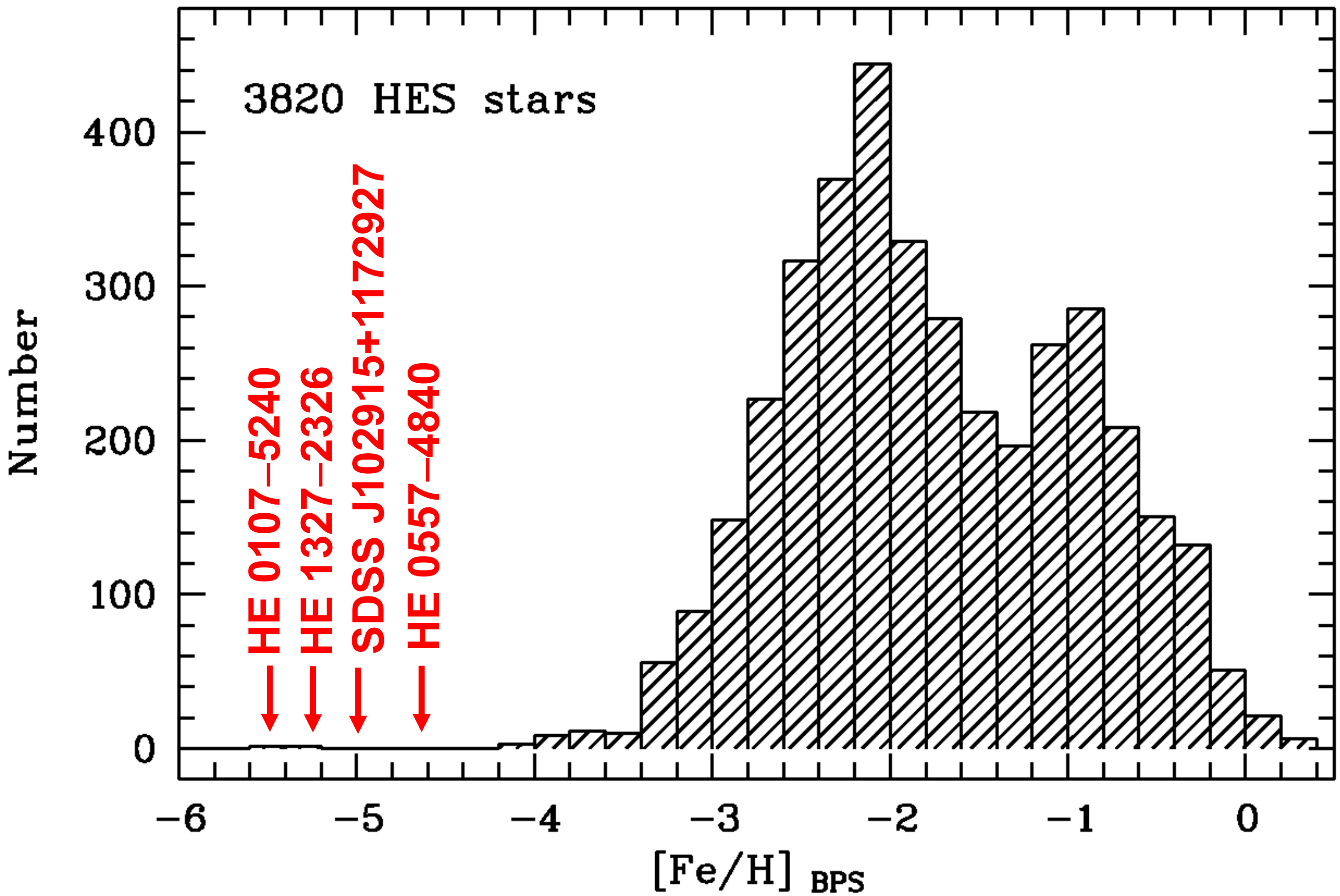

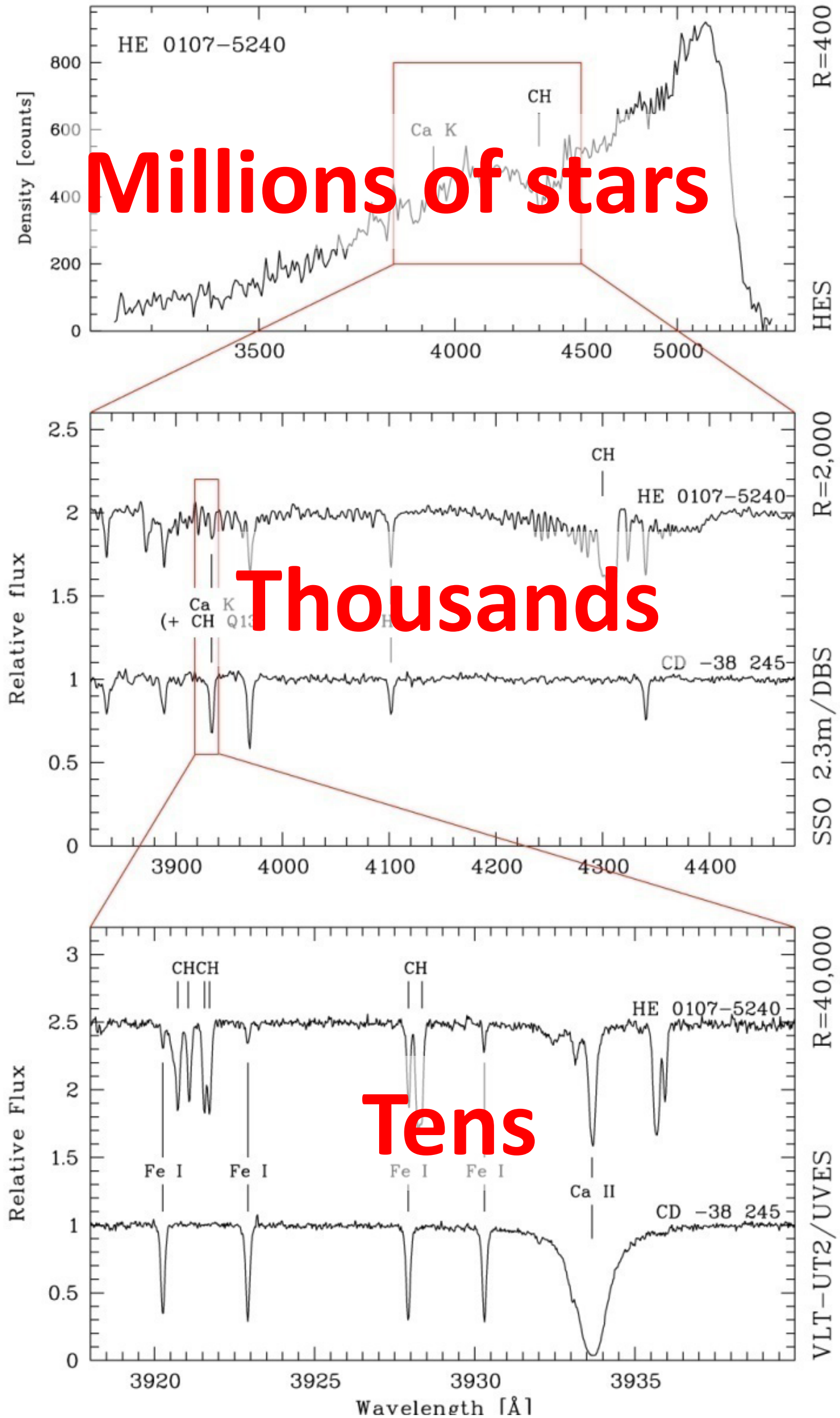

Photometry, or low resolution spectroscopy
($R = \lambda/\Delta\lambda \approx 10-1{,}000$)

Medium resolution spectroscopy
($R = \lambda/\Delta\lambda \approx 1{,}000-20{,}000$)

High resolution spectroscopy
($R = \lambda/\Delta\lambda > 20{,}000$)

How stars at [Fe/H] < –4.0 are hiding

- Contamination of Ca K with CH lines

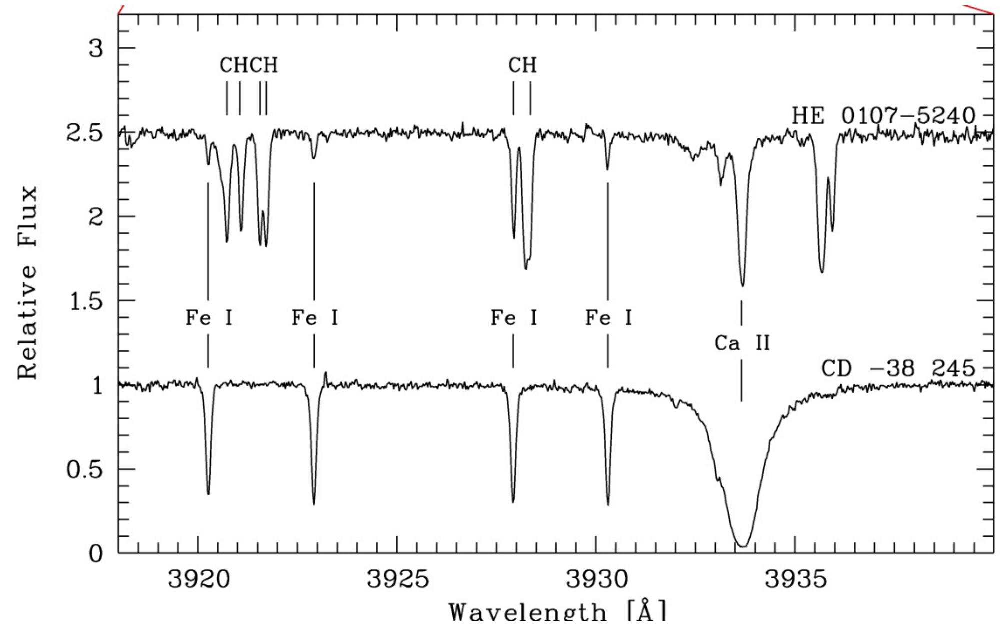

- [α/Fe] > +0.4?

- Contamination of Ca K with interstellar

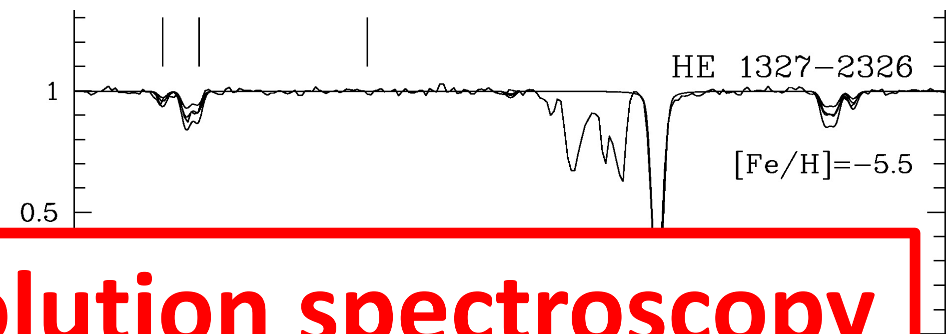

=> Need high-resolution spectroscopy of all stars at [Fe/H] < –3.5!

Past and present surveys

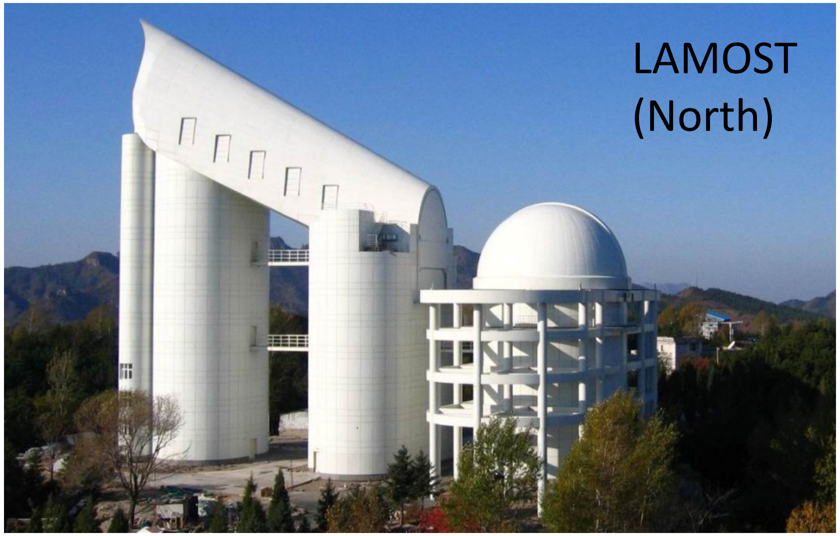

Survey	Effective sky coverage	Effective mag limit	*N* < –3.0 (EMP)	*N* < –5.0 (HMP)	People
HES	6,400 deg^2	*B* < 16.5	200	2	Christlieb et al.
SEGUE	1,000 deg^2	*B* < 19	(1,000)	(10)	Beers et al.; Caffau et al.
LAMOST	12,200 deg^2	*B* < 18.0	(3,000)	(30)	Zhao et al.
SSS	20,000 deg^2	*B* < 17.5	(2,500)	(25)	Keller et al.

LAMOST optical design

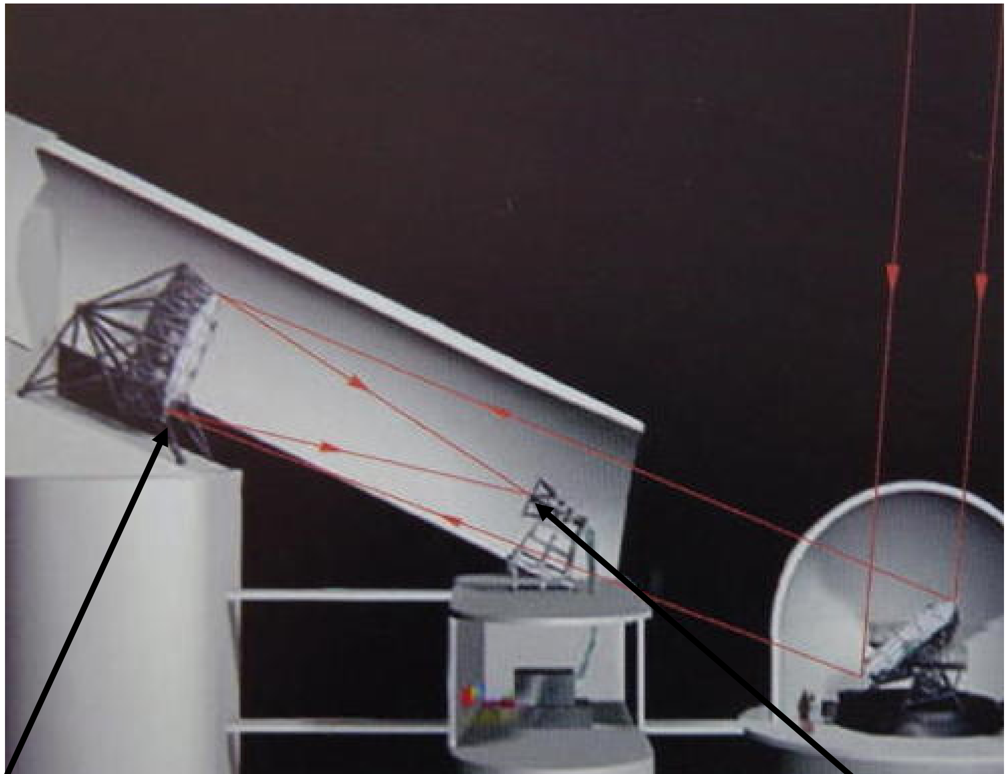

M_A
Reflecting Schmidt Corrector

M_B

Spherical "Primary" Mirror

Focal Plane

It's a meridian reflecting Schmidt telescope, laid down on the ground with its optical axis fixed in the meridian plane

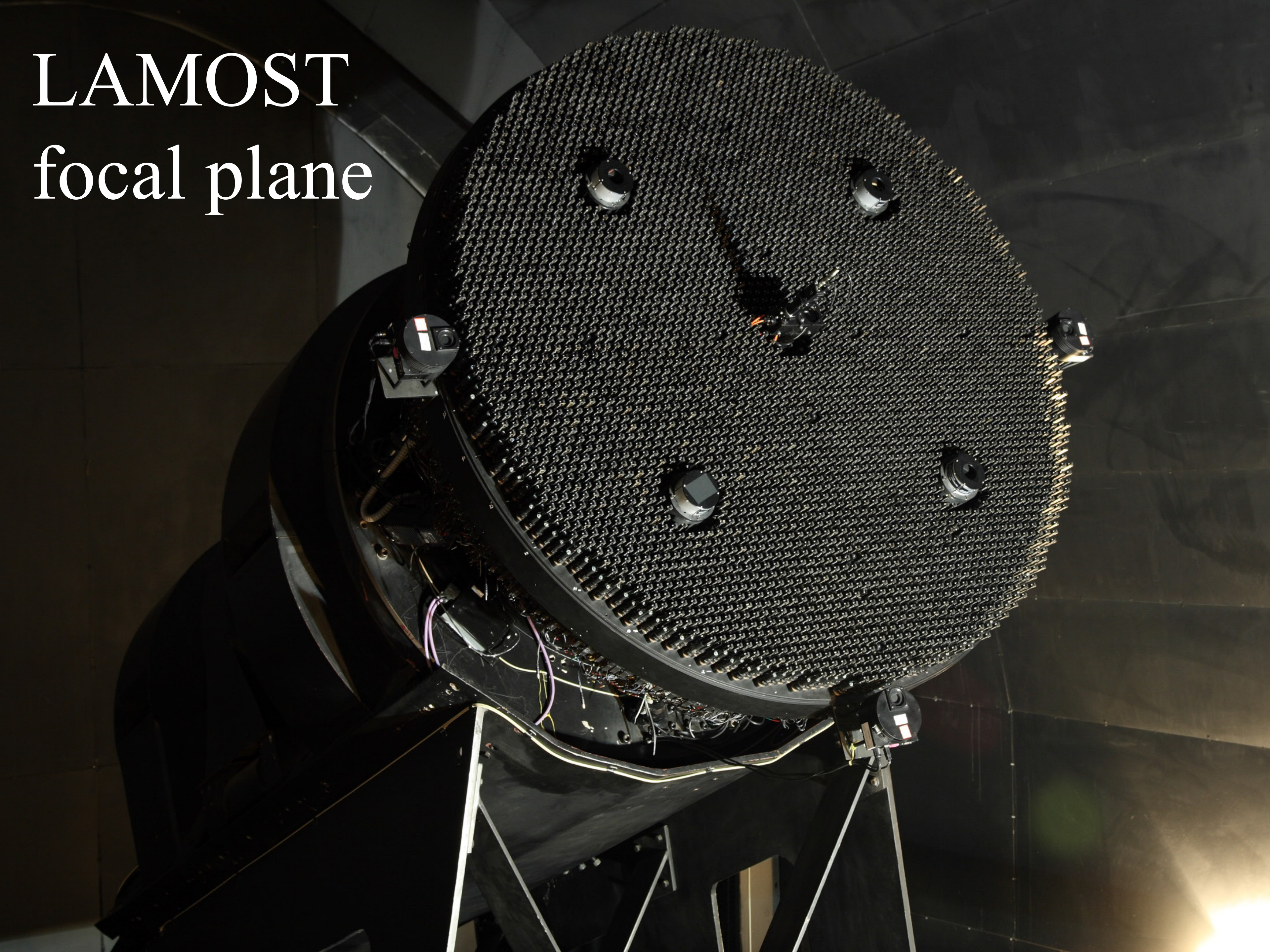
LAMOST
focal plane

LAMOST spectrograph configurations

Low-resolution mode

	Blue Arm		Red Arm	
	R	Wave. range (nm)	R	Wave. range (nm)
Full slit	1000	370-590	1000	570-900
1/2 slit	2000	370-590	2000	570-900

Medium-resolution mode

	Blue Arm		Red Arm	
	R	Wave. range (nm)	R	Wave. range (nm)
Full slit	5000	510-550	5000	830-890
1/2 slit	10000	510-550	10000	830-890

LAMOST metal-poor star survey

- Targets selected from SDSS photometry.
  - □ $0.1 < (g-r)_0 < 1.0$
  - □ $g < 18.0$
  - □ $|b| > 20°$, $Z > 5$ kpc
  - □ $-10° < \delta < 70°$

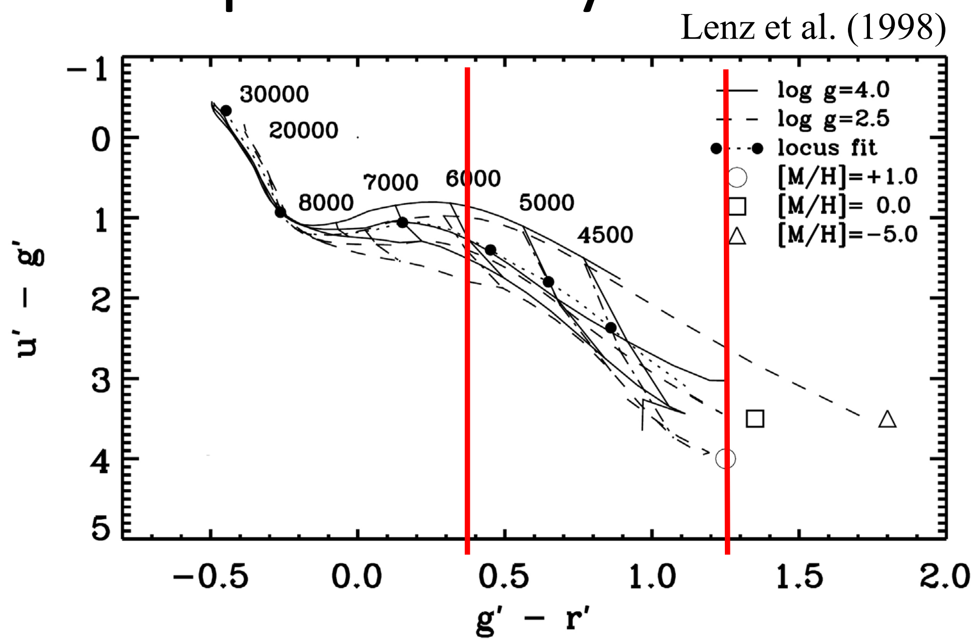

- Some 5 million stars selected; about 2 million expected to be observed in 5-year survey, which was started this year.
- Some 300,000 spectra observed during pilot survey already published.

Stars at [Fe/H] < –4.0

Star	T_{eff}	log *g*	[Fe/H]	[C/H]	[N/H]	[O/H]	[Mg/H]	[Sr/H]
HE 0233–0343	6100K	3.4	–4.7	–1.2			–4.1	–4.4
HE 0557–4840	4900K	2.2	–4.8	–3.1	< –3.8	–2.5	–4.5	< –5.8
HE 1327–2326	6180K	3.7	–5.7	–1.4	–1.1	–1.8	–3.9	–4.7
SDSS JXXXX+YYYY	6350K	4.0	–5.0?	–1.0				
HE 0107–5240	5100K	2.2	–5.4	–1.3	–3.0	–3.1	–5.1	< –5.8
SDSS J1029+1729	5800K	4.0	–4.7	< –3.8	< –4.1		–4.7	< –5.1
SM 0313–XXXX	[redacted]							

Note: These are 1D LTE abundances. 3D corrections for C, N, O are typically –0.5 to –1.0 dex.

References: T. Hansen et al. (2013, in prep.); Norris et al. (2008, ApJ 670, 774); Norris et al. (2010, ApJ 753, 150), Frebel et al. (2005, Nature 434, 871); Aoki et al. (2006, ApJ 639, 897); Frebel et al. (2006, ApJ 638, L17); Frebel et al. (2008, ApJ 684, 588); Bonifacio et al. (2013, in prep.); Christlieb et al. (2002, Nature 419, 904); Christlieb et al. (2004, ApJ 603, 708); Bessel et al. (2004, ApJ 612, L61); Caffau et al. (2011, Nature 477, 67); Caffau et al. (2012, A&A 542, A51); Keller et al. (2013, in prep.).

The abundance patterns of HE 0107–5240 and HE 1327–2326

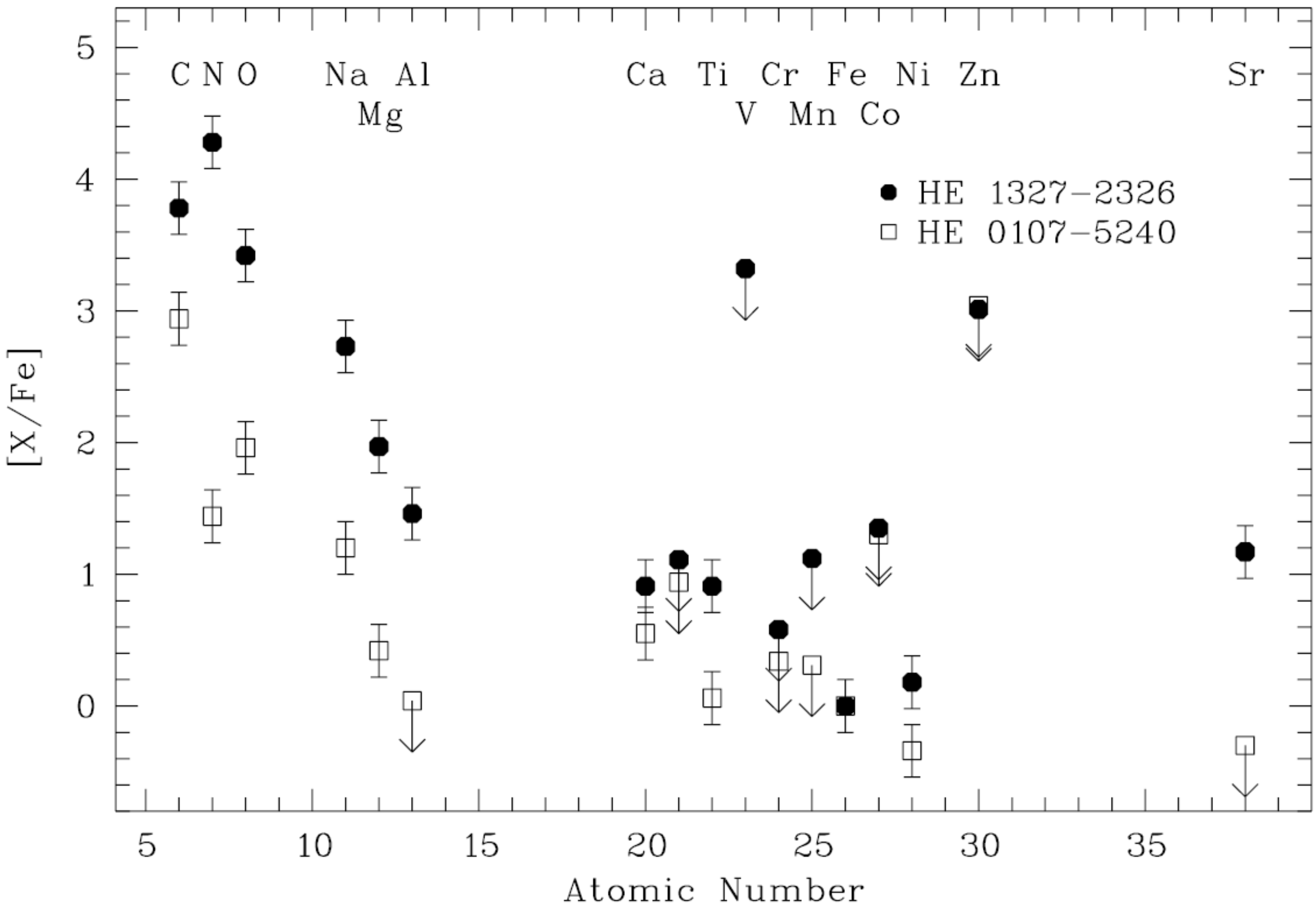

(Frebel et al. 2008, ApJ 684, 588)

Yields of fast-rotating, massive stars

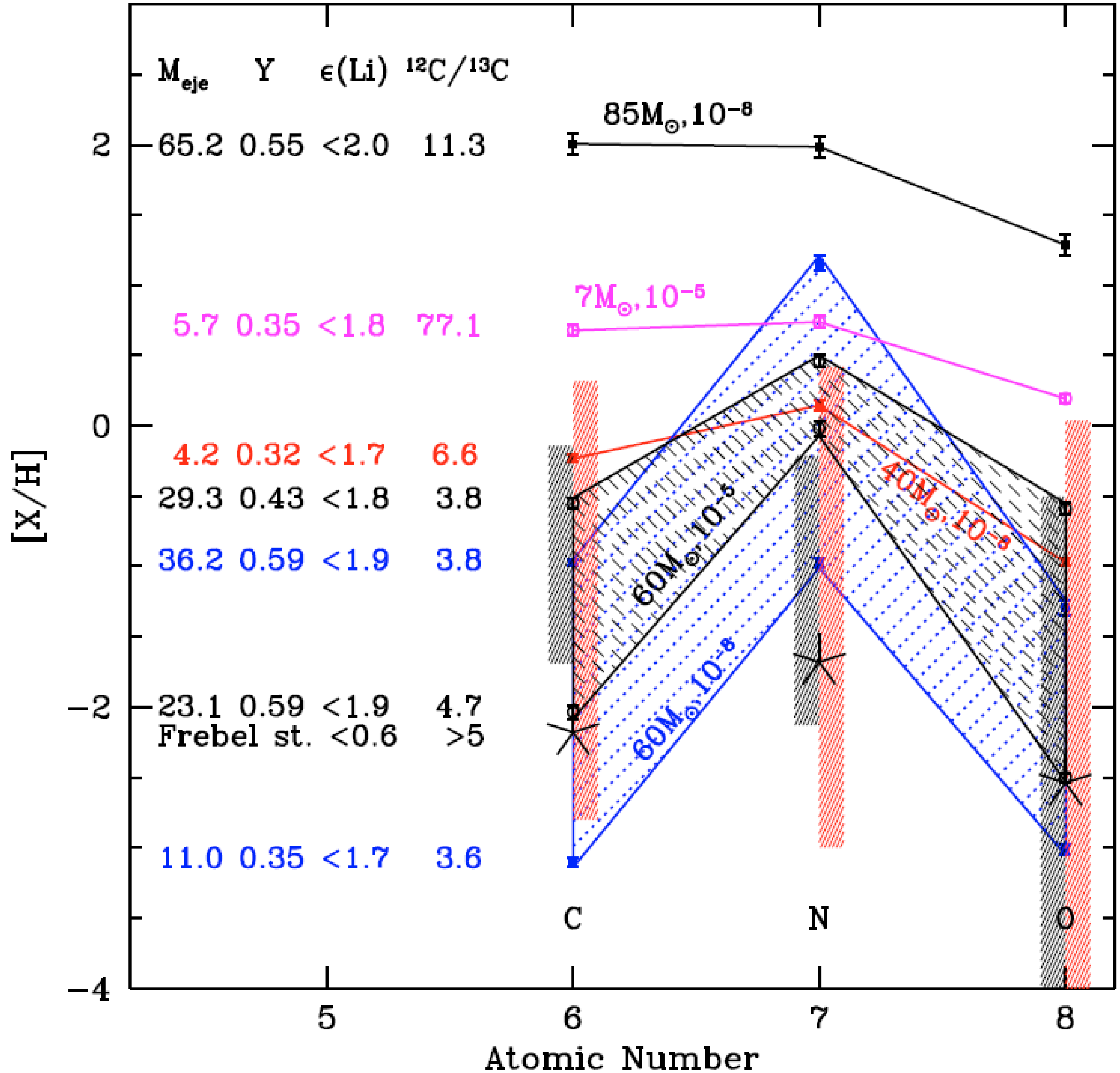

Meynet et al. (2010, A&A 521, A30)

Modeling the abundance patterns of HE 0107–5240 and HE 1327–2326 with mixing and fallback SN II

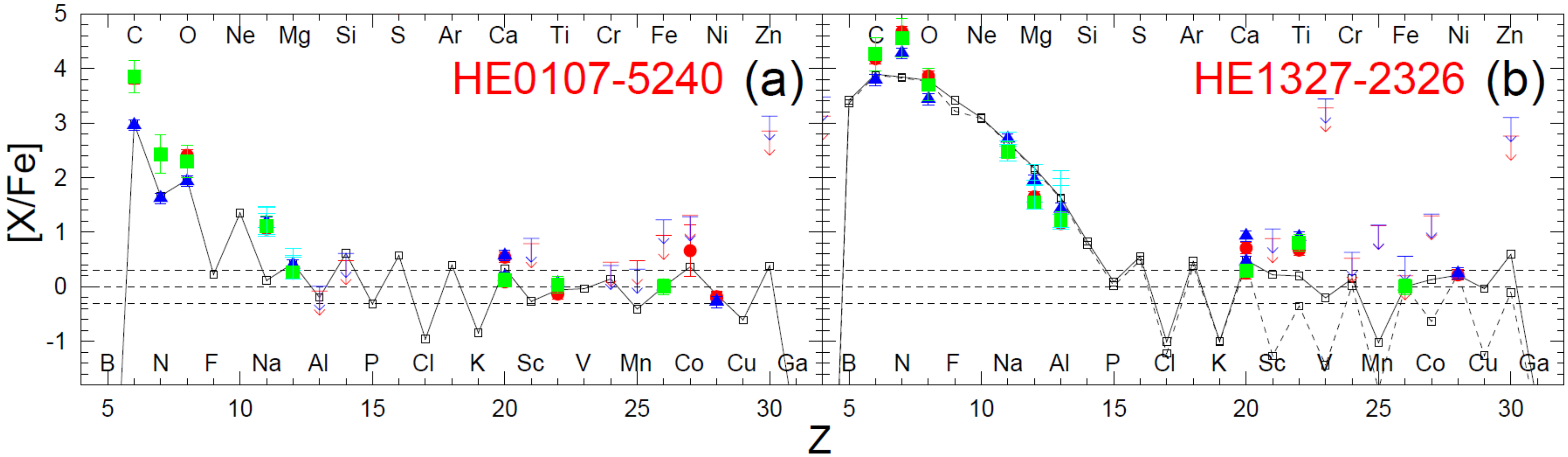

(Tominaga et al. 2013, submitted to ApJ, arXiv:1309.6734)

Quasar absorption line spectroscopy

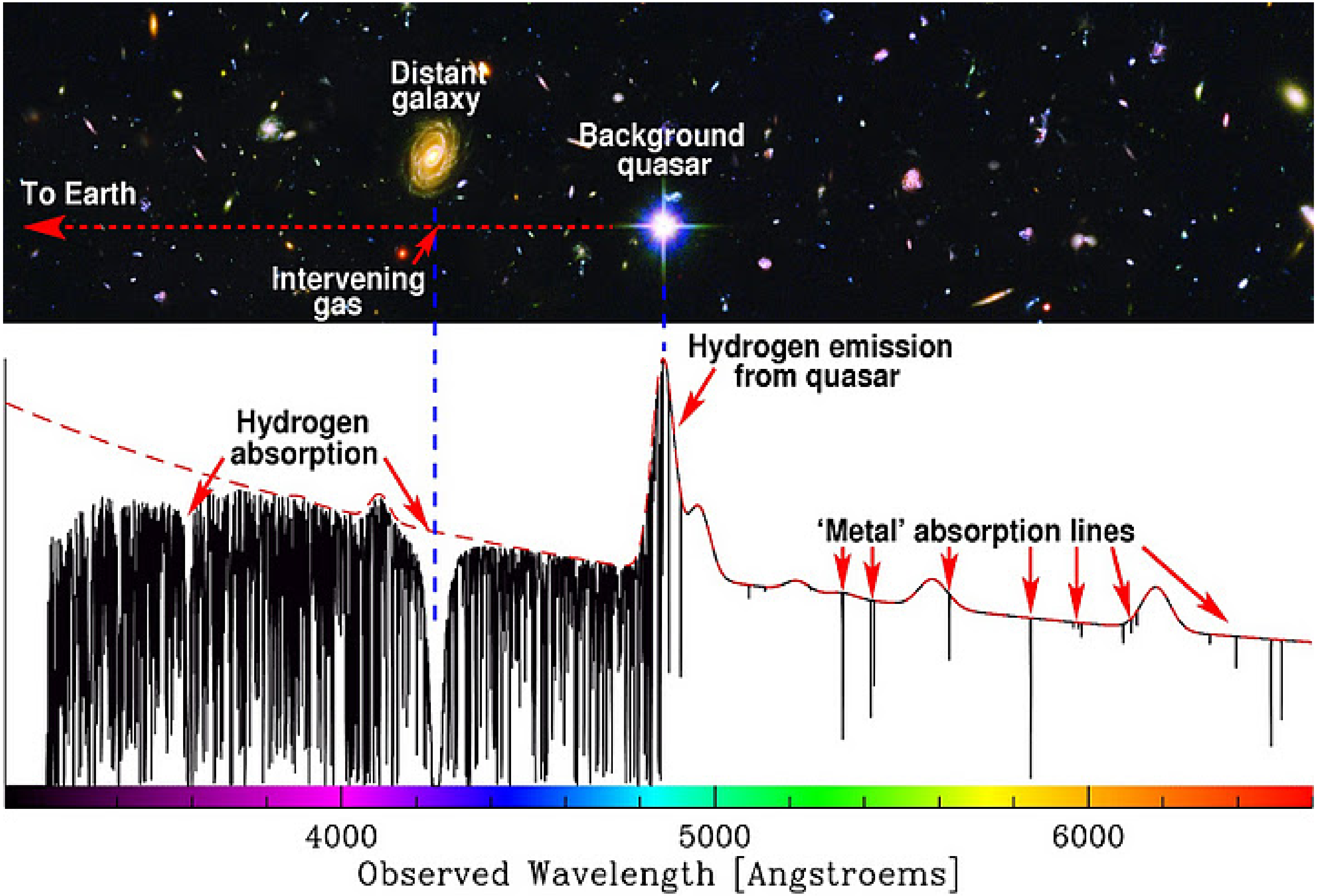

A damped Lyman-α system

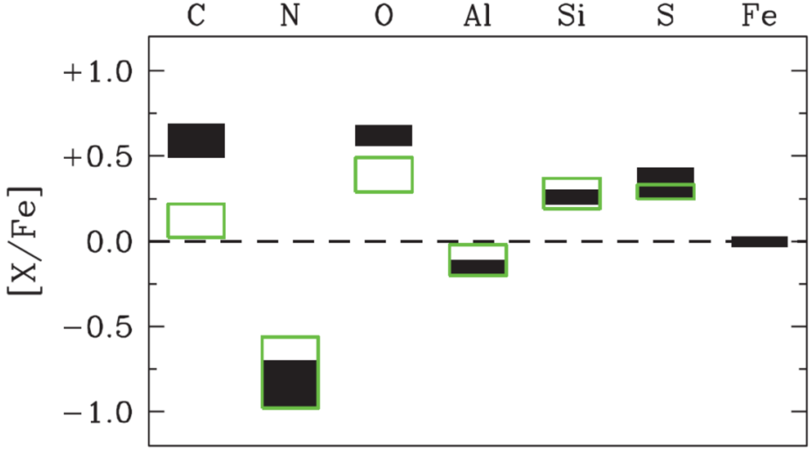

Cooke et al. (2012, 425, 347)

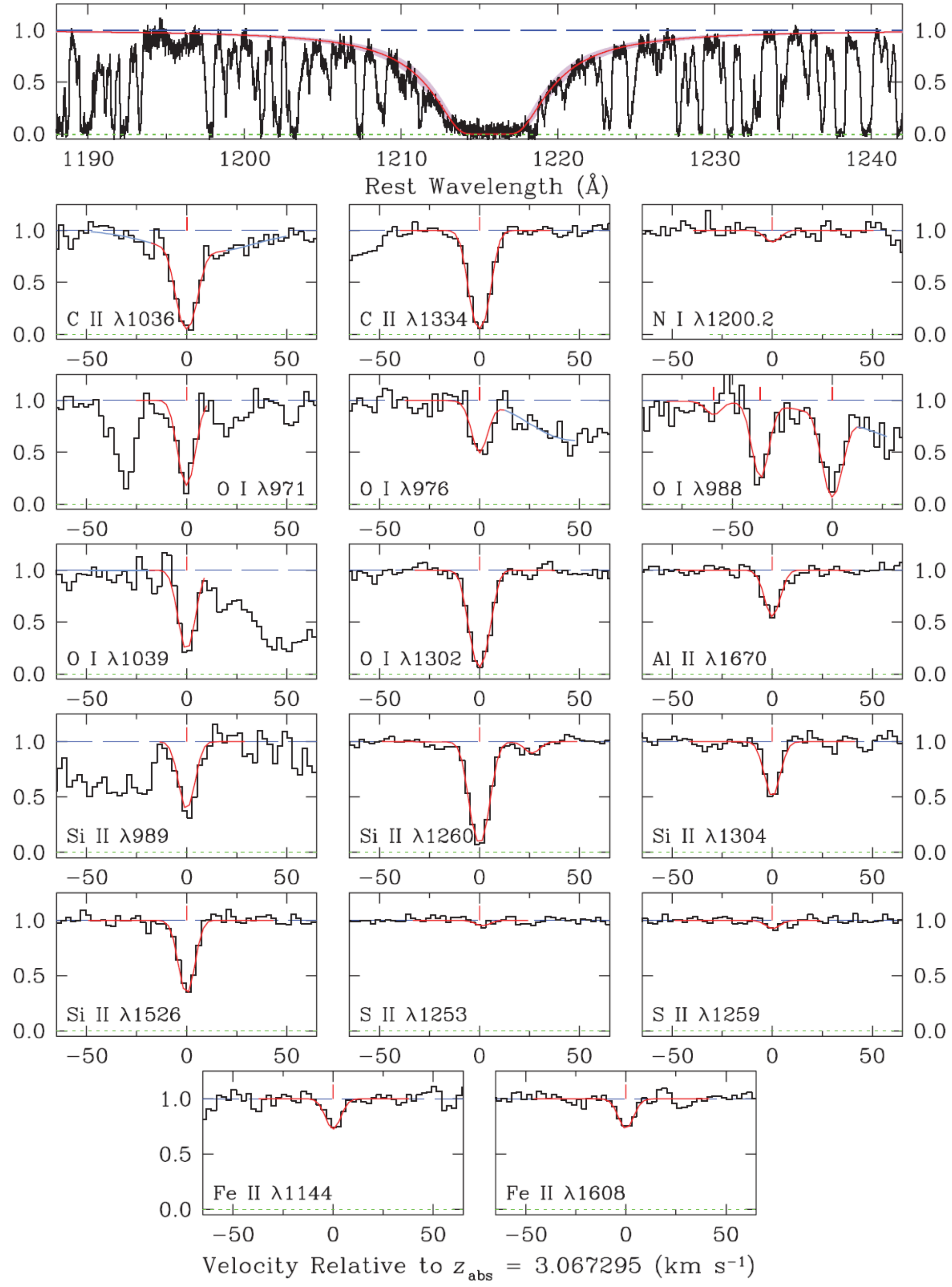

SDSS J102915+172927: a star in the heart of the lion

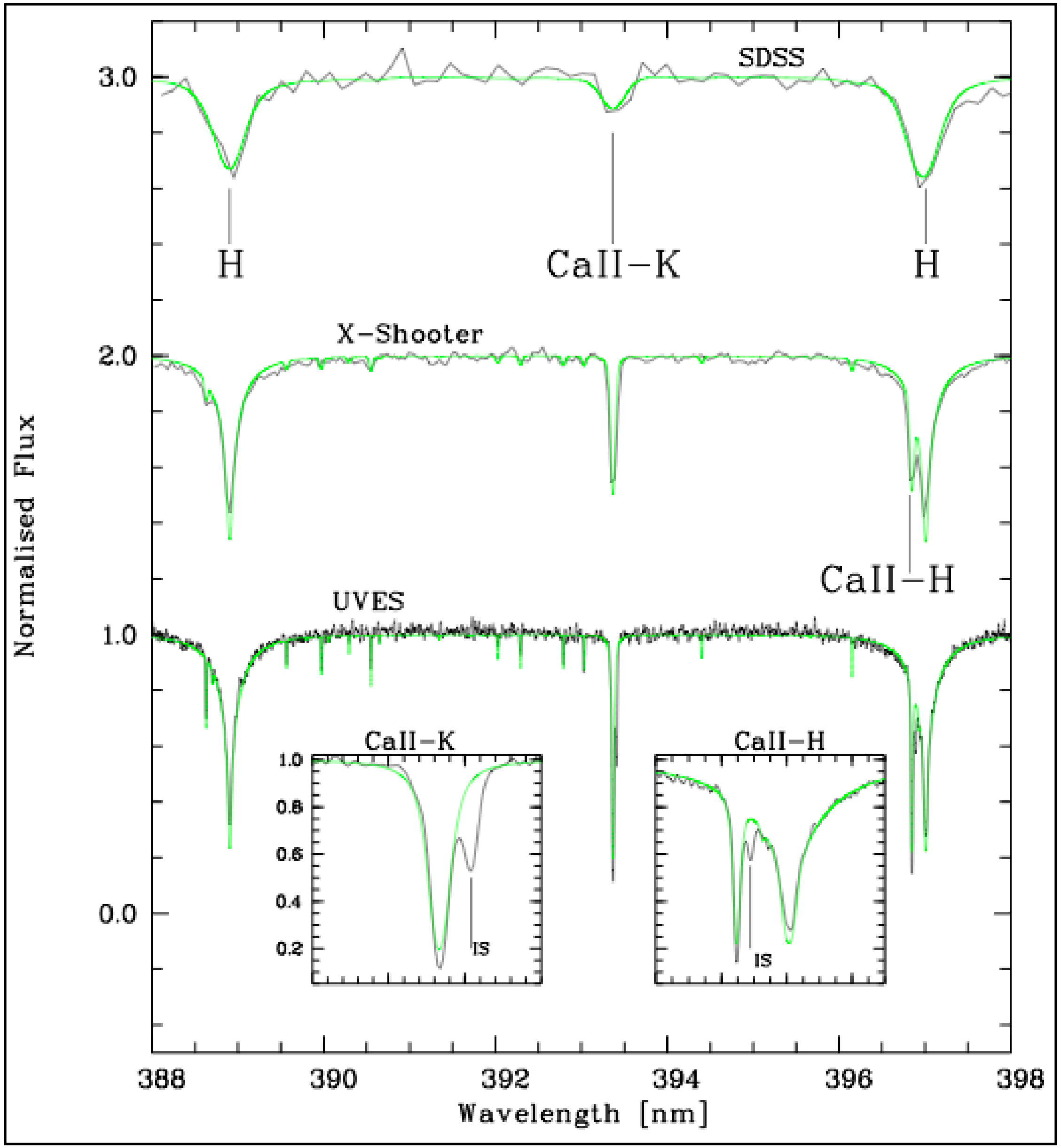

Caffau et al. (2011, Nature 477, 67)

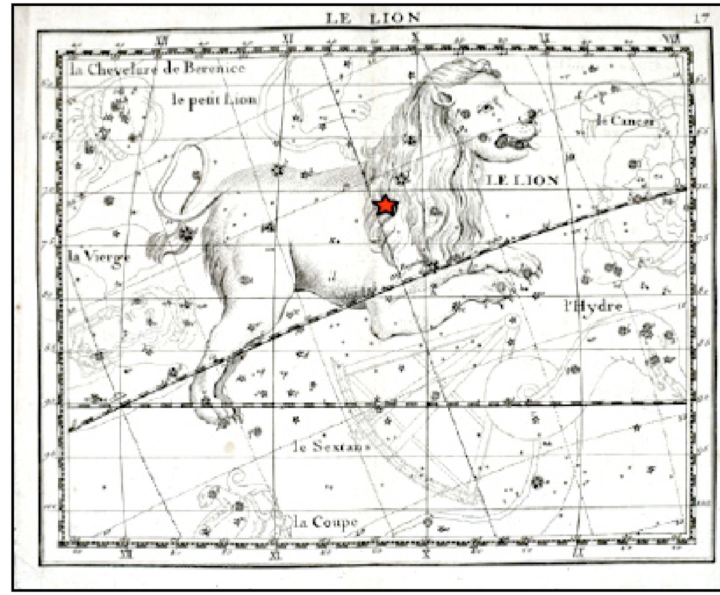

Star	SDSS J102915+172927
RA	10h 29m 15.15s
Dec	+17° 29′ 28″
u, mag	17.73
g, mag	16.92
r, mag	16.53
i, mag	16.41
z, mag	16.33
V_{rad}	-35.5
T_{eff}, [K]	5811
$\log g$	4.0
ξ, $km\,s^{-1}$	1.5
$[Fe/H]_{3D}$	−5

Abundances of the *most metal-poor* star

Element	A(X), 3D	[X/H], 3D	[X/Fe], 3D	[X/H], 1D	Number of lines	$A(X)_\odot$
C	≤ 4.2	≤ -4.3	$\leq +0.7$	≤ -3.8	G band	8.50
N	≤ 3.1	≤ -4.8	$\leq +0.2$	≤ -4.1	NH band	7.86
Mg I	2.95	-4.59 ± 0.10	+0.40	-4.68 ± 0.08	4	7.54
Si I	3.25	-4.27 ± 0.10	+0.72	-4.27 ± 0.10	1	7.52
Ca I	1.53	-4.80 ± 0.10	+0.19	-4.72 ± 0.10	1	6.33
Ca II	1.48	-4.85 ± 0.11	+0.14	-4.71 ± 0.11	3	6.33
Ti II	0.14	-4.76 ± 0.11	+0.23	-4.75 ± 0.11	6	4.90
Fe I	2.53	-4.99 ± 0.12	+0.00	-4.73 ± 0.13	44	7.52
Ni I	1.35	-4.88 ± 0.11	+0.11	-4.55 ± 0.14	10	6.23
Sr II	≤ -2.28	≤ -5.2	≤ -0.21	≤ -5.1	1	2.92

Caffau et al. (2011, Nature 477, 67)

Where is the carbon?

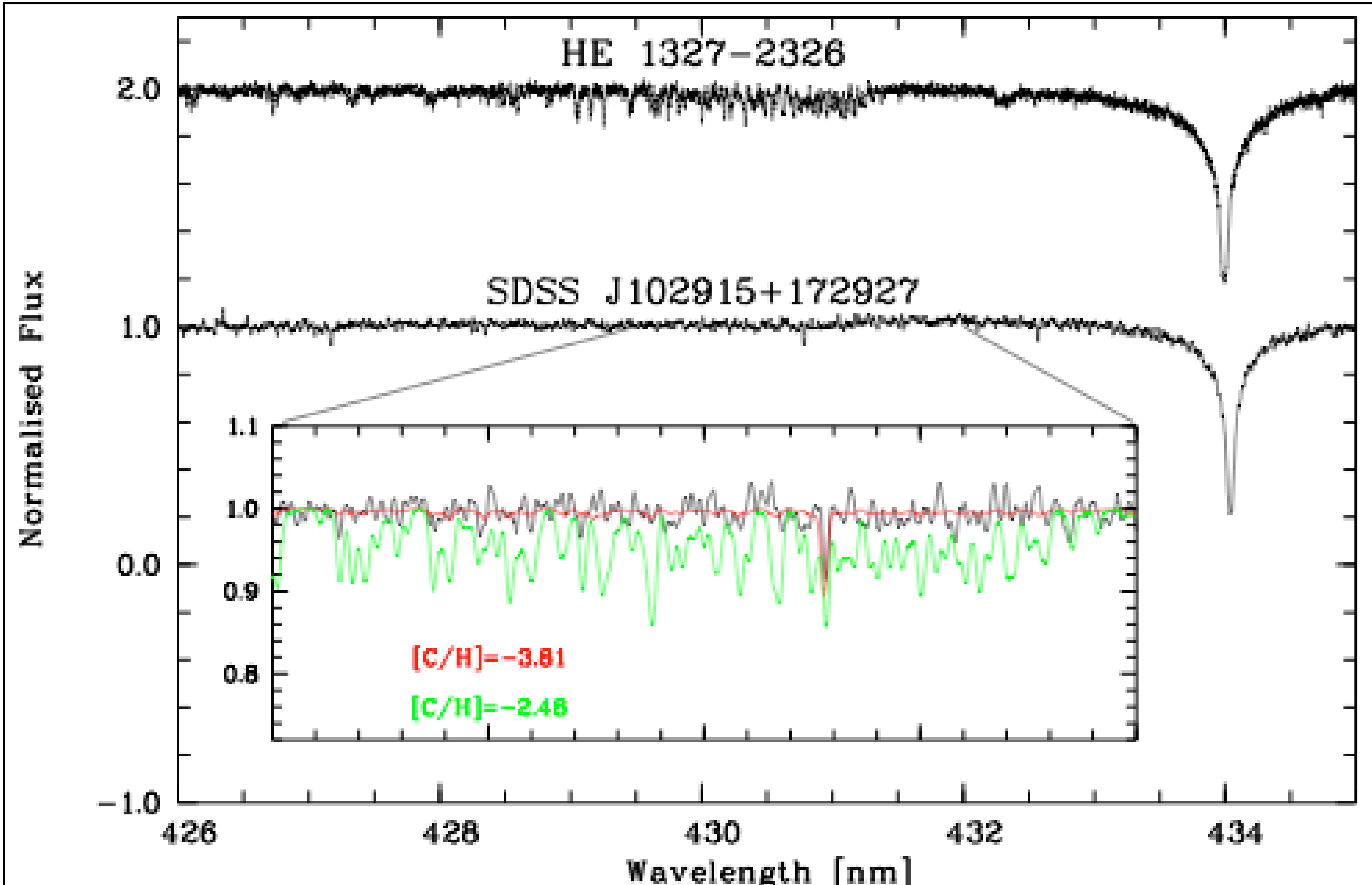

Entering the „forbidden zone“

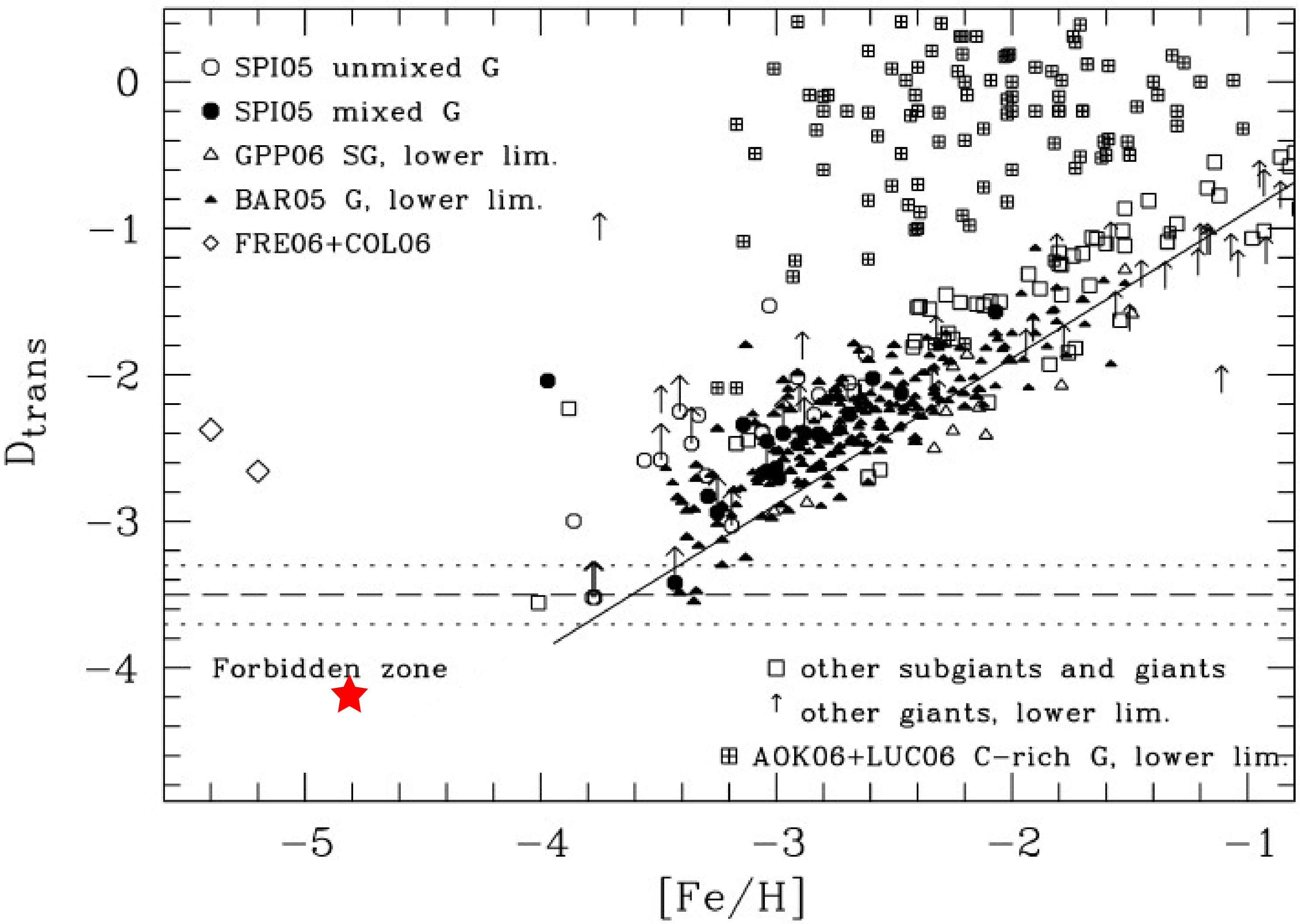

$D_{trans}=\log_{10}(10^{[C/H]}+0.3*10^{[O/H]})$ (Frebel et al. 2007)

Stars at [Fe/H] < –4.0

Star	T_{eff}	log *g*	[Fe/H]	[C/H]	[N/H]	[O/H]	[Mg/H]	[Sr/H]
HE 0233–0343	6100K	3.4	–4.7	–1.2			–4.1	–4.4
HE 0557–4840	4900K	2.2	–4.8	–3.1	< –3.8	–2.5	–4.5	< –5.8
HE 1327–2326	6180K	3.7	–5.7	–1.4	–1.1	–1.8	–3.9	–4.7
SDSS JXXXX+YYYY	6350K	4.0	–5.0?	–1.0				
HE 0107–5240	5100K	2.2	–5.4	–1.3	–3.0	–3.1	–5.1	< –5.8
SDSS J1029+1729	5800K	4.0	–4.7	< –3.8	< –4.1		–4.7	< –5.1
SM 0313–XXXX	[redacted]							

Note: These are 1D LTE abundances. 3D corrections for C, N, O are typically –0.5 to –1.0 dex.

References: T. Hansen et al. (2013, in prep.); Norris et al. (2008, ApJ 670, 774); Norris et al. (2010, ApJ 753, 150), Frebel et al. (2005, Nature 434, 871); Aoki et al. (2006, ApJ 639, 897); Frebel et al. (2006, ApJ 638, L17); Frebel et al. (2008, ApJ 684, 588); Bonifacio et al. (2013, in prep.); Christlieb et al. (2002, Nature 419, 904); Christlieb et al. (2004, ApJ 603, 708); Bessel et al. (2004, ApJ 612, L61); Caffau et al. (2011, Nature 477, 67); Caffau et al. (2012, A&A 542, A51); Keller et al. (2013, in prep.).

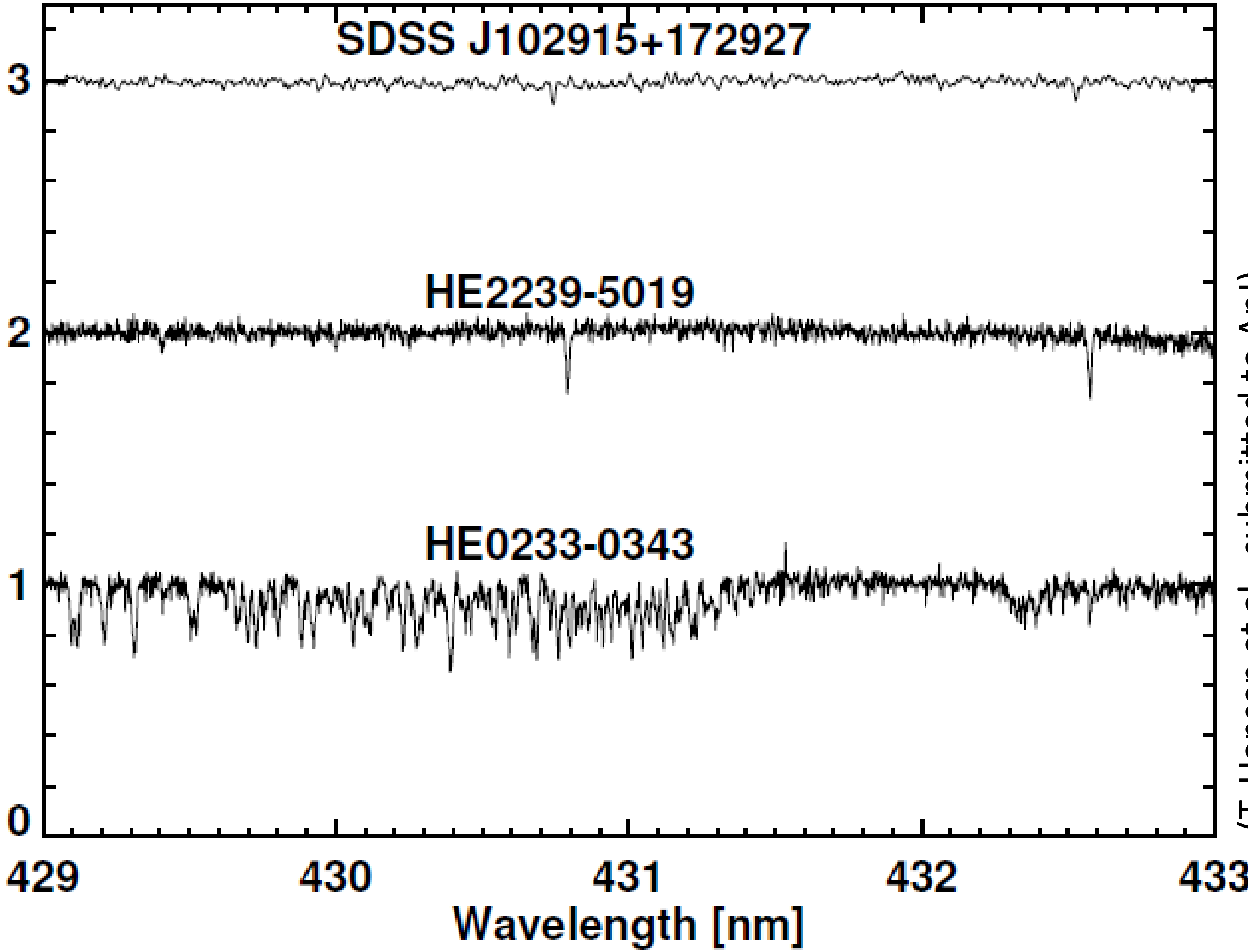

(T. Hansen et al., submitted to ApJ)

Strontium

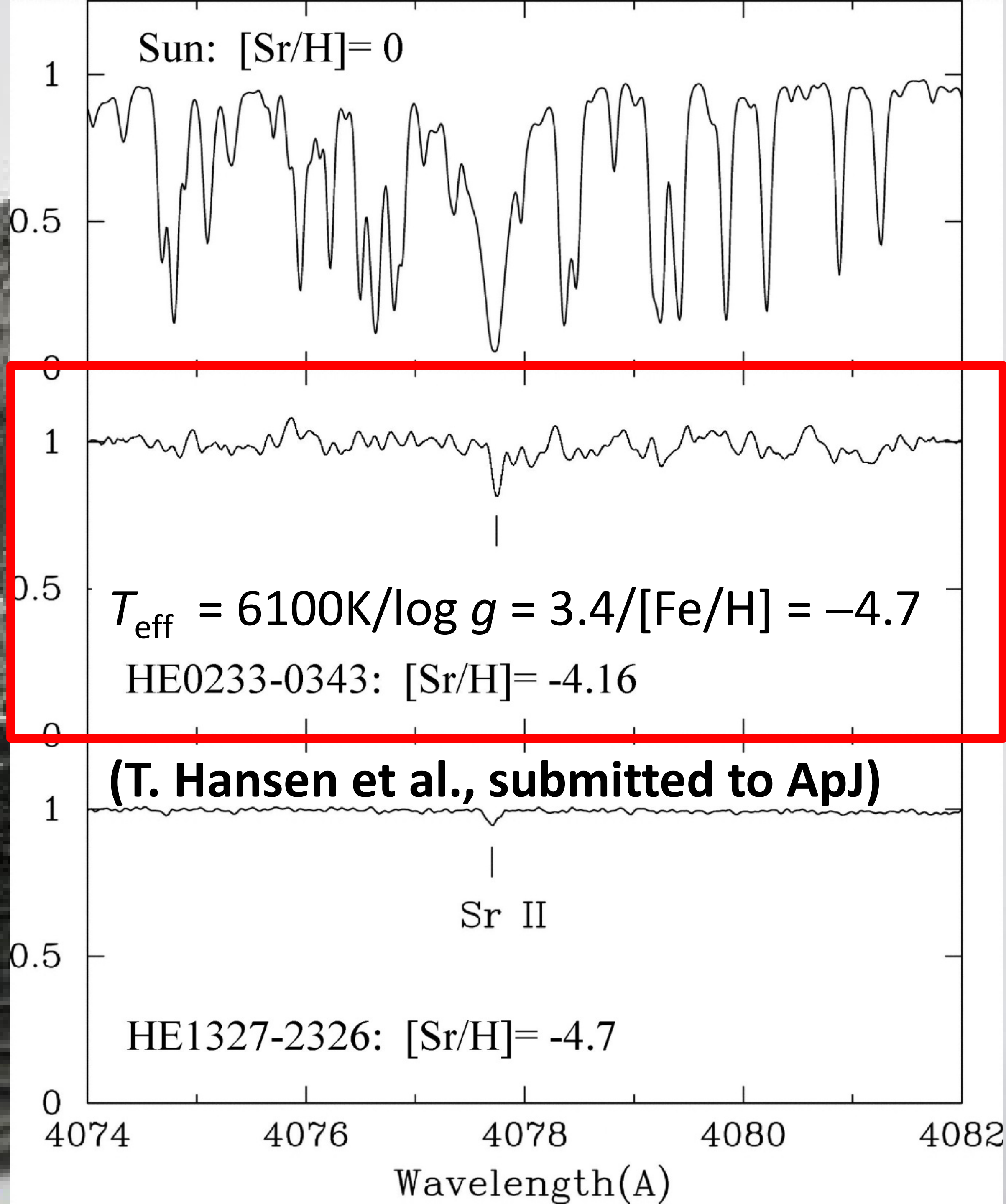

Sun: [Sr/H]= 0
T_{eff} = 6100K/log g = 3.4/[Fe/H] = –4.7
HE0233-0343: [Sr/H]= -4.16
(T. Hansen et al., submitted to ApJ)
Sr II
HE1327-2326: [Sr/H]= -4.7
1
0.5
0
4074
4076
4078
4080
4082
Wavelength(A)

Abundances of HE 0233–0343

$\log \epsilon(\mathrm{Li})$	1.77 (0.18)
[C/Fe]	3.46 (0.24)
[N/Fe]	<1.80 ···
[Na/Fe]	<0.50 ···
[Mg/Fe]	0.59 (0.15)
[Al/Fe]	<0.03 ···
[Si/Fe]	0.37 (0.15)
[Ca/Fe]	0.34 (0.15)
[Sc/Fe]	<0.20 ···
[Ti/Fe]	0.18 (0.17)
[Cr/Fe]	<0.50 ···
[Mn/Fe]	<−0.10 ···
[Co/Fe]	<1.60 ···
[Ni/Fe]	<0.90 ···
[Sr/Fe]	0.32 (0.19)
[Ba/Fe]	<0.80 ···

(T. Hansen et al., submitted to ApJ)

[Sr/Ba]

Star	**[Sr/Ba]**	**Star type**
HD 122563	+0.76	weak r-process star
HE 1327−2326	**> −0.2**	
HE 0233−0343	**> −0.4**	
CS 31082−001	−0.52	r-II star
CS 22892−052	−0.41	r-II star
CS 29497−004	−0.46	r-II star
HE 0024−2523	−1.12	CEMP-s star
LP 625-44	−1.59	CEMP-s star

Conclusion: Sr in HE 1327−2326 and HE 0233−0343 was not made by *main* s-process, but most likely by the weak r-process.

Are there any stars without neutron-capture elements?

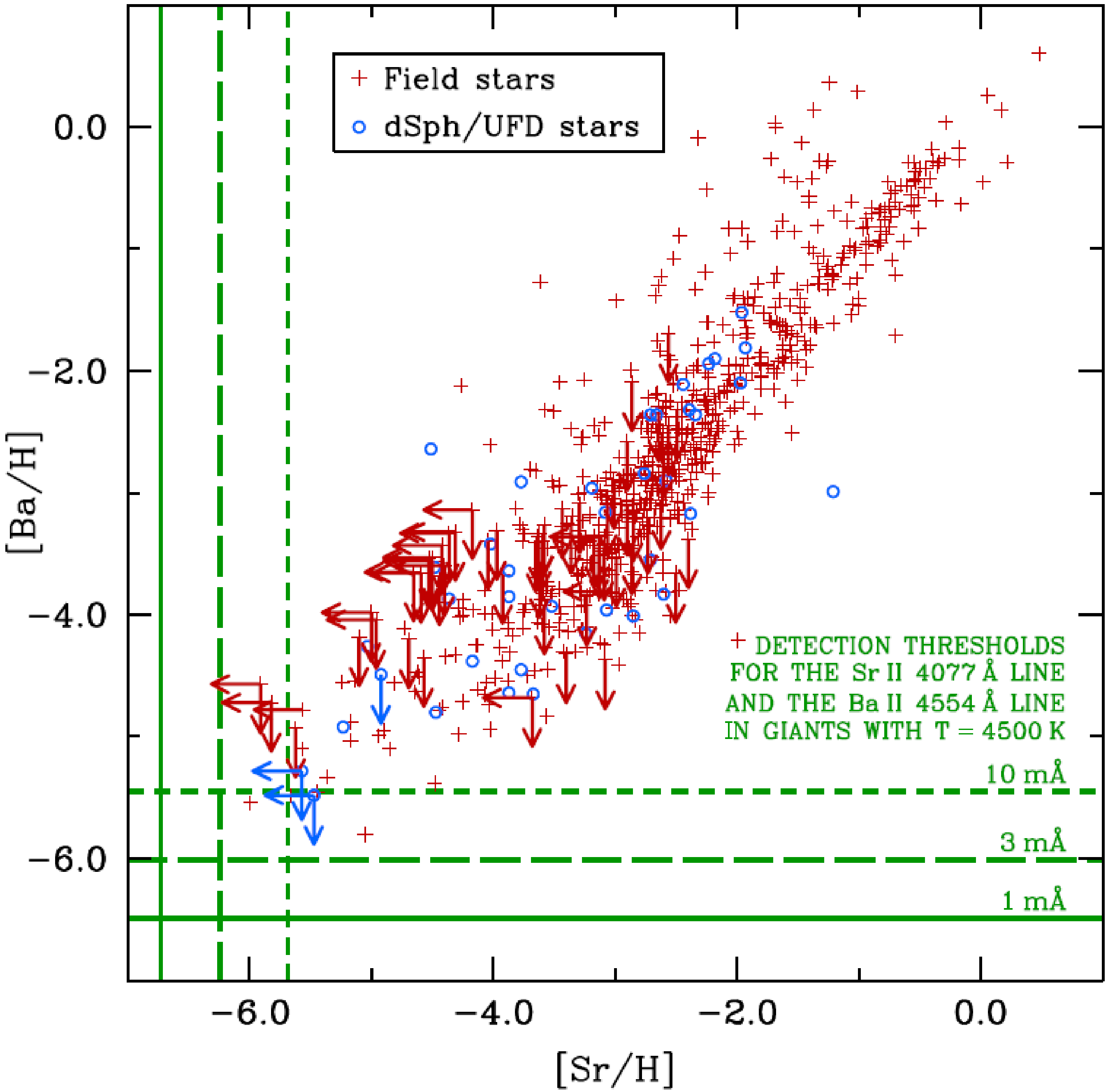

(Roederer 2013, AJ 145, 26)

Kinematics, and Gaia

Kinematics: Toomre diagram

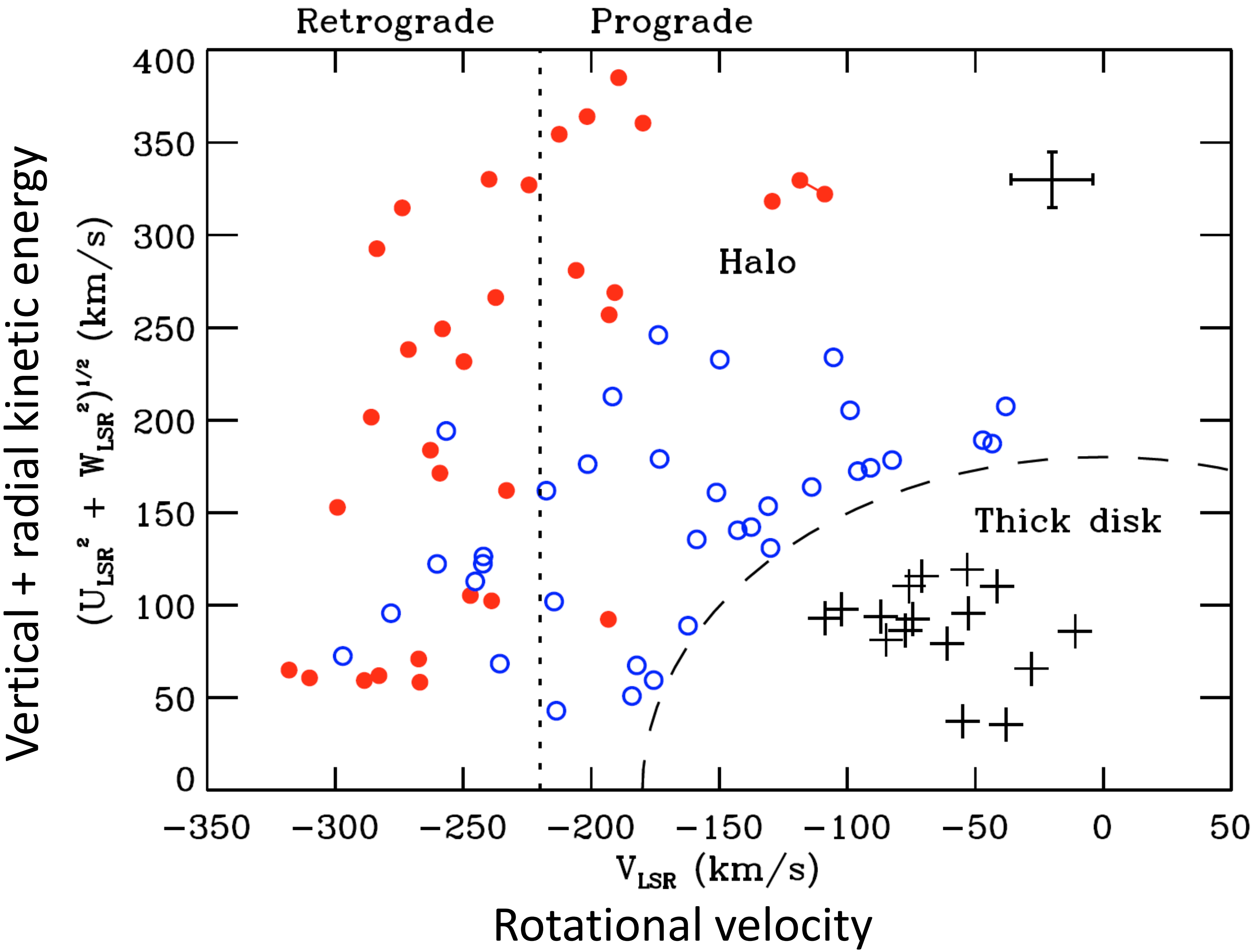

Low-α vs. high-α stars

(Nissen & Schuster 2010, A&A 511, L10)

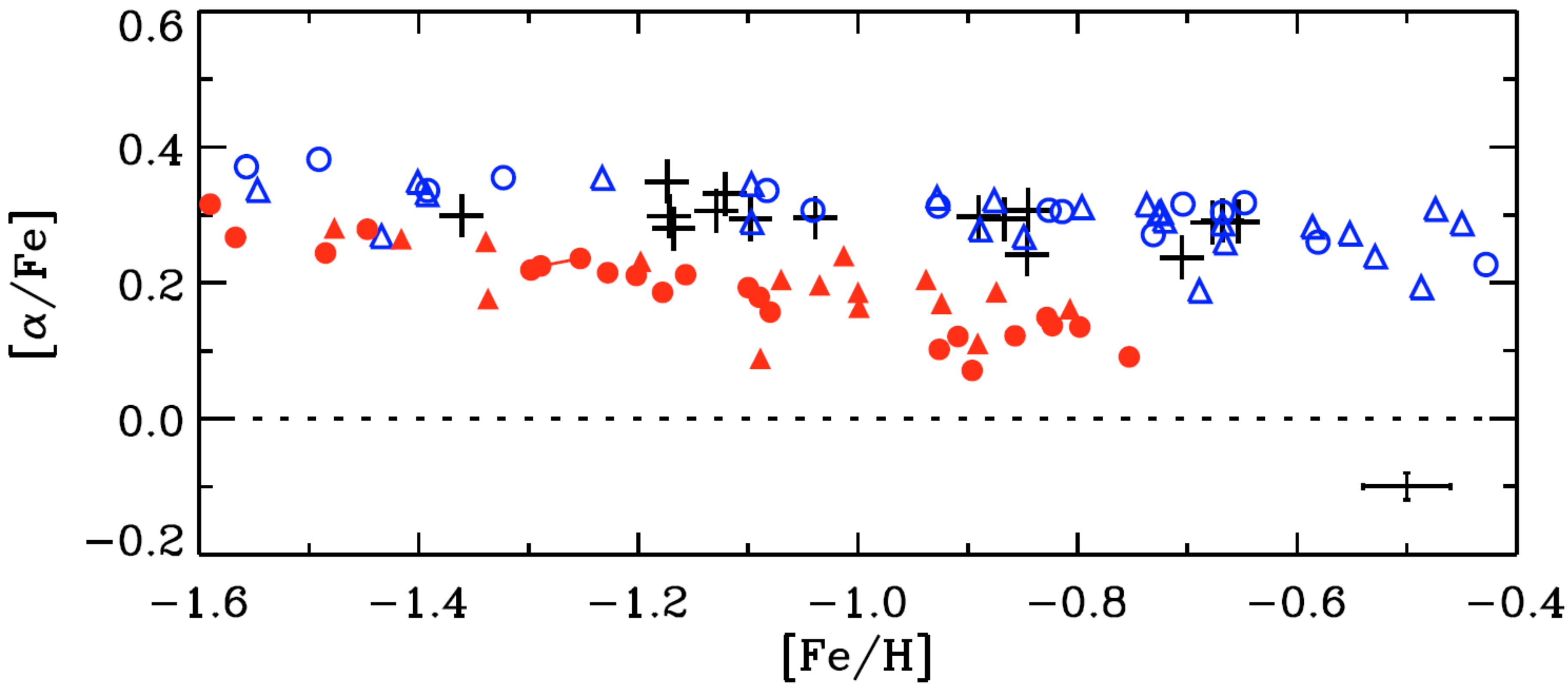

Gaia timeline

- Launch: currently planned for 18 December 2013.
- First data release
  - September 2015 (launch + 22 months)
  - Positions with sub-mas accuracy for 90% of the sky
  - G magnitudes
  - Improved proper motions for Hipparcos stars
- Second data release
  - **March 2016** (launch + 28 months)
  - Based on 15 months of observations = 1/3 of mission duration; 90% sky coverage
  - G magnitudes, spectrophotometry
  - **Positions, parallaxes: sqrt(3) · σ_{final}**
  - **Proper motions: sqrt(6) · σ_{final}**
- Final data release: ~2020

Conclusions

- The abundance patterns of the most metal-poor stars are the imprints of the earliest chemical enrichment events in the Universe. We can derive from them properties of the first generation of stars, and study the physics of star formation in metal-poor environments.
- The currently ongoing, wide-angle sky surveys for metal-poor/iron-deficient stars are expected to increase the samples by at least one order of magnitude.
- Stellar abundances combined with kinematics from Gaia will allow us to reconstruct how the Galaxy formed.